



Optimum satellite remote sensing of the marine carbonate system using empirical algorithms in the global ocean, the Greater Caribbean, the Amazon Plume and the Bay of Bengal

Peter E. Land^{a,*}, Helen S. Findlay^a, Jamie D. Shutler^b, Ian G.C. Ashton^b, Thomas Holding^b, Antoine Grouazel^c, Fanny Girard-Arduin^c, Nicolas Reul^c, Jean-Francois Piolle^c, Bertrand Chapron^c, Yves Quilfen^c, Richard G.J. Bellerby^{d,e}, Punyasloke Bhadury^f, Joseph Salisbury^g, Douglas Vandemark^g, Roberto Sabia^h

^a Plymouth Marine Laboratory, Prospect Place, West Hoe, Plymouth, PL1 3DH, UK

^b University of Exeter, Penryn, Cornwall, TR10 9FE, UK

^c Ifremer, University Brest, CNRS, IRD, Laboratoire d'Océanographie Physique et Spatiale (LOPS), IUEM, F-29280, Brest, France

^d SKLEC-NIVA Centre for Marine and Coastal Research, State Key Laboratory for Estuarine and Coastal Research, East China Normal University Zhongshan N. Road, 3663, Shanghai, 200062, China

^e Norwegian Institute for Water Research, Thormøhlensgate 53D, N-5006, Bergen, Norway

^f Department of Biological Sciences, Indian Institute of Science Education and Research Kolkata, Mohanpur, 741 246, West Bengal, India

^g Ocean Processes Analysis Laboratory, University of New Hampshire, Durham, NH, 3824, United States

^h Telespazio-Vega U.K. for European Space Agency (ESA), ESRIN, Frascati, Italy

ARTICLE INFO

Keywords:

Carbonate chemistry
Earth observation
Ocean acidification
Total alkalinity
Dissolved inorganic carbon
SMOS
Aquarius
CORA
HadGEM2-ES

ABSTRACT

Improving our ability to monitor ocean carbonate chemistry has become a priority as the ocean continues to absorb carbon dioxide from the atmosphere. This long-term uptake is reducing the ocean pH; a process commonly known as ocean acidification. The use of satellite Earth Observation has not yet been thoroughly explored as an option for routinely observing surface ocean carbonate chemistry, although its potential has been highlighted. We demonstrate the suitability of using empirical algorithms to calculate total alkalinity (A_T) and total dissolved inorganic carbon (C_T), assessing the relative performance of satellite, interpolated *in situ*, and climatology datasets in reproducing the wider spatial patterns of these two variables. Both A_T and C_T *in situ* data are reproducible, both regionally and globally, using salinity and temperature datasets, with satellite observed salinity from Aquarius and SMOS providing performance comparable to other datasets for the majority of case studies. Global root mean squared difference (RMSD) between *in situ* validation data and satellite estimates is $17 \mu\text{mol kg}^{-1}$ with bias $< 5 \mu\text{mol kg}^{-1}$ for A_T and $30 \mu\text{mol kg}^{-1}$ with bias $< 10 \mu\text{mol kg}^{-1}$ for C_T . This analysis demonstrates that satellite sensors provide a credible solution for monitoring surface synoptic scale A_T and C_T . It also enables the first demonstration of observation-based synoptic scale A_T and C_T temporal mixing in the Amazon plume for 2010–2016, complete with a robust estimation of their uncertainty.

1. Introduction

The oceans play an important role in absorbing carbon (e.g. Sabine et al., 2004), and the increase in CO_2 emitted into the atmosphere as a result of anthropogenic activities has resulted in an increase in CO_2 uptake by the oceans (Caldeira and Wickett, 2005; Sabine et al., 2004; Takahashi et al., 2009). This long-term absorption results in a shift in ocean carbonate chemistry, which has the potential to alter biogeochemical cycles and ecosystem function in the future (Raven et al.,

2005; Kroeker et al., 2013). As a result of the decrease in ocean pH arising from these shifts (often termed Ocean Acidification), this change in ocean carbonate chemistry has received increasing scientific and political attention over the past decade. This has led to questions about the magnitude and importance of spatial and temporal ocean carbon variability, as well as how to monitor ongoing change at global and regional scales. To-date, carbonate system monitoring has been primarily from ship- and field-based observations that provide relatively disparate and sparse datasets of carbonate chemistry parameters in both

* Corresponding author.

E-mail address: peland@pml.ac.uk (P.E. Land).

<https://doi.org/10.1016/j.rse.2019.111469>

Received 12 February 2019; Received in revised form 20 September 2019; Accepted 10 October 2019

Available online 08 November 2019

0034-4257/ © 2019 Published by Elsevier Inc.

space and time. To expand capabilities, state-of-the-art autonomous *in situ* tools are needed (Byrne, 2014). Recent advances include pH sensors on biogeochemical floats (e.g. Johnson et al., 2017), and sensors to observe multiple carbonate system parameters *in situ* are now in development (Bushinsky, 2019). One such advancement is utilizing Earth Observation (EO) satellites to provide wider spatial and temporal coverage of surface carbonate chemistry observations, with the aim of detecting features and characterizing dynamics that are difficult to resolve using *in situ* datasets (Land et al., 2015; Salisbury et al., 2015; Fine et al., 2017). Currently, there are just two satellites in orbit that are specifically designed to support global carbon cycle research (The US NASA Orbiting Carbon Observatory OCO-2 (Osterman et al., 2016), and the Chinese Tansat; Yang et al., 2018), but their focus is to observe and monitor atmospheric CO₂. However, there is a suite of ocean observing satellite sensor datasets that could be used, through exploitation of empirical relationships, to provide measures of marine carbonate chemistry parameters that include total alkalinity (A_T), total dissolved inorganic carbon (C_T), partial pressure of CO₂ in seawater (pCO₂) and pH (Gledhill et al., 2009).

These four primary variables allow the ocean carbonate system to be investigated. In principle, knowledge of at least two of these four, in conjunction with temperature, salinity and pressure, allows the remaining variables to be calculated (Dickson and Riley, 1978). The relationships between these variables are principally driven by thermodynamics; temperature, pressure and salinity are therefore fundamentally associated with the carbonate system (Dickson et al., 2007). Furthermore, salinity is a significant driver of the ionic composition of seawater and hence has a strong relationship with A_T (Millero et al., 1998). In addition to these physical controls on the carbonate system, the variables can be influenced by other chemical processes, including weathering and carbonate formation/dissolution (Friis et al., 2003), and biological processes such as primary production, respiration, calcification and remineralization (Smith and Key, 1975). With this knowledge it is possible to determine how the carbonate system variables vary in relation to factors such as temperature, salinity, nitrate or chlorophyll (the latter two as proxies for biological processes). These relationships take the form of empirical algorithms, which can be used to derive the respective carbonate system variable, and have been developed within a number of global and regional studies, e.g. Takahashi and Sutherland, 2013; Lee et al. (2006); Lee et al. (2000); Sasse et al. (2013); Cai et al. (2010); Lefèvre et al. (2010); Bonou et al. (2016); see Land et al. (2015) and references therein.

Although initially developed from *in situ* datasets, these empirical algorithms could potentially be forced with inputs from other sources, such as satellite observations or climatologies to yield observation-based carbon system observations. Here we conduct a first assessment of four global algorithms for A_T and three for C_T, utilizing different combinations of satellite, interpolated *in situ* and climatology datasets as input. We then evaluate their output using independent *in situ* measurements of A_T and C_T. As a baseline comparison, we evaluate estimates of A_T and C_T from an Earth System model. In addition to the global algorithms, we also assess three regional A_T and two regional C_T algorithms. We aim to demonstrate algorithm suitability both globally and for regional case studies (the Caribbean, the Amazon plume and the Bay of Bengal), and to assess the performance of these different approaches, particularly the relevance of satellite datasets, in being able to reproduce the *in situ* patterns of these two carbonate system variables in surface waters.

2. Materials and methods

2.1. Published algorithms

The four global algorithms used here for A_T are from Lee et al. (2006) (hereafter referred to as L06), Takahashi and Sutherland (2013) (hereafter referred to as TS13) and Sasse et al. (2013) (domain-based

and global algorithms, hereafter referred to as S13 and S13g). L06 separated the oceans into five domains and used an optimal polynomial fit to A_T data, resulting in a relationship with sea surface salinity (SSS) and sea surface temperature (SST) for each region. TS13 took this a step further using a larger combination of datasets to separate the oceans into 33 domains. Instead of using SST and SSS, TS13 assessed potential alkalinity relationship with SSS, where potential alkalinity is A_T plus nitrate concentration (NO₃), which corrects A_T for the effect of changes in NO₃ caused by net community utilization. Sasse et al. (2013) used multiple linear regression to relate domain and global A_T to SST, SSS, SSS², dissolved oxygen (DO), silicate (Si) and phosphate (PO₄). The three regional A_T algorithms are all linear relationships with SSS using data from the Amazon plume and Caribbean (Cai et al., 2010; Lefèvre et al., 2010). Two other regional algorithms (Cooley et al., 2007; Ternon et al., 2000) were considered, but were not used here as results differed only marginally from Lefèvre et al. (2010) and they used much of the same training data.

The three global C_T algorithms that we used are from Lee et al. (2000) (hereafter referred to as L00) and Sasse et al. (2013) (domain-based and global algorithms, hereafter referred to as S13 and S13g). L00 found C_T normalized to salinity 35 on the Practical Salinity Scale and year 1990, ($nC_T = C_T \times 35 / SSS + (\text{year} - 1990)$ between 30°S and 30°N), to be strongly correlated with SST and NO₃, and conducted optimal polynomial fitting for C_T to domain data, giving a total of 12 regionally parameterized equations. Sasse et al. (2013) used multiple linear regression to relate domain and global C_T to SST, SSS, DO, NO₃, Si and PO₄. The two regional C_T algorithms are both linear relationships with SSS using data from the Amazon plume (Lefèvre et al., 2010; Bonou et al., 2016). The same two regional studies as for A_T (Cooley et al., 2007; Ternon et al., 2000) were considered for C_T, but again results differed only marginally from those of Lefèvre et al. (2010) and so they were not used.

In all cases, extrapolation of algorithms beyond the range for which they were calibrated is questionable, and this is especially true of nonlinear algorithms. To avoid this, we did not use any algorithm outside its specified range of applicability, or more than one SSS unit or SST degree outside its calibration range if a range of applicability is not specified. Table 1 summarises the algorithm choices and dependences. Additional details on each empirical relationship for all algorithms are provided in Supporting Information Text S1.

2.2. Round-robin comparison

Four case study regions were used in a round-robin comparison of the algorithms: the global ocean, the Caribbean (14°N to 30°N, 90°W to

Table 1

Summary of algorithms, their dependencies and the region for which they were originally developed. AT = Total Alkalinity, CT = Dissolved Inorganic Carbon; SSS = Sea Surface Salinity, SST = Sea Surface Temperature, DO = Dissolved Oxygen, N = nitrate, Si = silicate, P = phosphate.

Product	Name	Dependencies	Reference	Region
AT	TS13	SSS, N	Takahashi and Sutherland (2013)	Global
AT	L06	SSS, SST	Lee et al. (2006)	Global
AT	S13	SSS, SST, DO, Si, P	Sasse et al., (2013)	Global
AT	S13g	SST, SSS, DO, Si, P	Sasse et al., (2013)	Global
AT		SSS	Lefèvre et al. (2010)	APR
AT		SSS	Cai et al. (2010)	GCR, APR
CT	L00	SSS, SST, N	Lee et al. (2000)	Global
CT	S13	SST, SSS, DO, N, Si, P	Sasse et al., (2013)	Global
CT	S13g	SST, SSS, DO, N, Si, P	Sasse et al., (2013)	Global
CT		SSS	Lefèvre et al. (2010)	APR
CT		SSS	Bonou et al. (2016)	APR

60°W for compatibility with Gledhill et al. (2008)), the Amazon plume (2°S to 22°N, 70°W to 32°W), and the Bay of Bengal (5°N to 24°N, 78°E to 96°E, using the Bay of Bengal International Hydrographic Office Sea Area (International Hydrographic Organization, 1953)). These case studies were chosen as areas that are potentially challenging for this assessment and are discussed in more detail in Land et al. (2015). The Amazon region was chosen to enclose the region of freshening contiguous with the mouth of the Amazon with any monthly satellite SSS < 35, with an eastern boundary at 32°W, beyond which rain freshening dominates the Amazon plume (Ibáñez et al., 2016). The region defined also includes many points with SSS > 35. To investigate the effect of these points, we also defined a low-salinity Amazon region where data with *in situ* SSS > 35 were excluded.

Each algorithm was tested using input data for each forcing factor (SSS, SST, NO₃, DO, Si and/or PO₄) from a range of data sources and all possible combinations of inputs were included in the round-robin comparison. The input data for the empirical algorithms were:

- 1) Monthly mean satellite observed data from the Soil Moisture and Ocean Salinity (SMOS) satellite [SSS 2010–2017 CATDS-IFR-CEC-v02] (Reul et al., 2015), the Aquarius satellite [SSS 2011–2015, Version 5] (Le Vine et al., 2014), and the Climate Change Initiative (CCI) [SST 1991–2010] (Merchant et al., 2012);
- 2) *In situ* re-analysis data from the Coriolis Ocean Re-Analysis (CORA v4.3) database [SSS, SST 1990–2012] (Cabanes et al., 2013);
- 3) Monthly climatology data from the World Ocean Atlas (WOA) dataset [SSS, SST, nitrate, DO, Si, PO₄] (Garcia et al., 2014a; Garcia et al., 2014b; Locarnini et al., 2013; Zweng et al., 2013); Note that WOA 'nitrate' is actually nitrate + nitrite (NO₃ + NO₂). However, NO₂ typically has a concentration at least an order of magnitude lower than NO₃, and so this discrepancy is neglected. The previously mentioned baseline comparison dataset were A_T and C_T output from the HadGEM2-ES global Earth system model, 1972–2020 (Jones et al., 2011) (hereafter referred to as HG2).

All data were binned spatially to a 1° × 1° grid and temporally to monthly intervals (henceforth referred to as monthly data). The multi-year CORA, satellite and HG2 data were also each combined to form monthly climatologies (climatological data). Only 1° × 1° grid cells with at least two values were used to calculate climatological data. Details of all of these input datasets are provided in Table 2.

The binned A_T or C_T from each algorithm and input, herein referred to as 'output', and the binned output from HG2 were all evaluated (validated) against binned *in situ* data of the respective carbonate parameter. Data from the Global Data Analysis Project Version 2 (GLODAPv2, 1972–2013) (Olsen et al., 2016) were the primary *in situ* evaluation (validation) data used for both A_T and C_T evaluations, along with some additional regional *in situ* data (see Table 3). The GLODAPv2 dataset is a community compiled, merged and internally consistent global dataset. In all cases of *in situ* data, the mean measurement in the top 10 m water depth was used.

Following (Sasse et al., 2013), we attempted to separate the effects of terrigenous influences and sediment resuspension on the biogeochemistry of coastal waters from open ocean carbonate chemistry by calculating the minimum depth within each cell using the GEBCO_08 1-min grid (www.gebco.net/data_and_products/gridded_bathymetry).

Table 2

Datasets used as inputs to the empirical algorithms. SSS = sea surface salinity, SST = sea surface temperature, DO = dissolved oxygen.

Type	Name	Time period	References	
SSS	Satellite	SMOS (CATDS v2)	2010 - 2014	Reul and Team (2015)
SSS	Satellite	Aquarius	2011 - 2014	Le Vine et al. (2014)
SST	Satellite	ESA SST CCI	1992 - 2010	Merchant et al. (2012)
SSS, SST	Re-analysis	CORA v4.0	1990 - 2012	Cabanes et al. (2013)
SSS, SST, DO, N, P, Si	Climatology	WOA	1970 - 2012	(Garcia et al., 2014a; Garcia et al., 2014b; Locarnini et al., 2013; Zweng et al., 2013)

Table 3

In situ carbonate chemistry datasets used for evaluating the outputs. All datasets for each variable were combined into one dataset that was averaged monthly on a 1° × 1° grid. The Bhadury et al. coastal data are from a sampling station located on the coast of India at 21° 40' 40.6" N, 88° 9' 19.2"E, shown in Fig. 1 of Choudhury et al. (2015) (Station 3). The Findlay et al. research cruise data are from cruises off the Svalbard and Greenland coasts, 78° 53'-59' N, 11° 42'-12' 27' E and 70° 14-49' N, 22° 4-32'W respectively.

Dataset name	Time period	References	
AT, CT	GLODAPv2	1970–2013	Olsen et al. (2016)
AT, CT	OWS Mike	2001 - 2007	Findlay et al., 2008
AT	Bhadury et al. coastal data	2014	Choudhury et al. (2015)
AT, CT	Findlay et al. research cruise	2012–2014	[Findlay pers. comm.]

[data/gebco_one_minute_grid/](http://data.gebco.net/data_and_products/gridded_bathymetry/), downloaded on December 14th, 2009) and repeating our analysis using only grid cells with minimum depth greater than 500 m. Again following (Sasse et al., 2013), we further separated terrigenous effects by calculating the minimum distance from the nearest coast within each cell using (<https://oceancolor.gsfc.nasa.gov/docs/distfromcoast/>, downloaded on October 5th, 2018) and repeated the analysis using only grid cells with both a minimum depth greater than 500 m and a minimum distance greater than 300 km. All three sets of results are included in Supplementary Information, but only data with both masks applied are presented here.

2.3. Statistical measures

2.3.1. Data uncertainties

The GLODAPv2 analysis (Olsen et al., 2016), the chosen reference validation dataset, includes an estimate of the maximum bias that exists between different instruments determined via a crossover analysis as 4 and 6 μmol kg⁻¹ for C_T and A_T respectively. Whereas a full uncertainty budget (i.e. a type A uncertainty estimate (BIPM, 2008) comprising a combination of bias and standard deviation of all measurements against a traceable standard) is not provided. Therefore in the absence of all components of the uncertainty information we assume nominal uncertainties of 0.5% for all *in situ* A_T and C_T (Bockmon et al., 2015). It should be noted that due to relatively recent improvements in quality control we would expect older *in situ* measurements to have greater uncertainties and more recent measurements to have lesser, though this variation is difficult to quantify. For interest, the GLODAPv2 bias estimate stated above for a mean global A_T of 2450 μmol kg⁻¹ gives a potential bias around 0.2%. Uncertainties in the input (forcing) data (SST, SSS, NO₃ and HG2 A_T and C_T) were not included in our analysis, since these are unknown for many of the input datasets. For interest only, the reported uncertainty in SMOS SSS is below ± 0.3 for a 30 day average over a 100 × 100 km open ocean area (Reul et al., 2012, 2014) and can be below ± 0.2 for an 18 day average (Boutin et al., 2018) or in certain evaporation-dominated regions, and for Aquarius SSS it is ± 0.17 for a monthly average over a 150 × 150 km open ocean area (Lagerloef et al., 2015). Uncertainty in CCI SST is between ± 0.1 and ± 0.15 K (Merchant et al., 2014). However, we could find no uncertainty estimates for the CORA, WOA or HG2 datasets, and it would be inconsistent to apply uncertainties to some inputs and not others. We discuss the impact of this approach within Section 4.2.

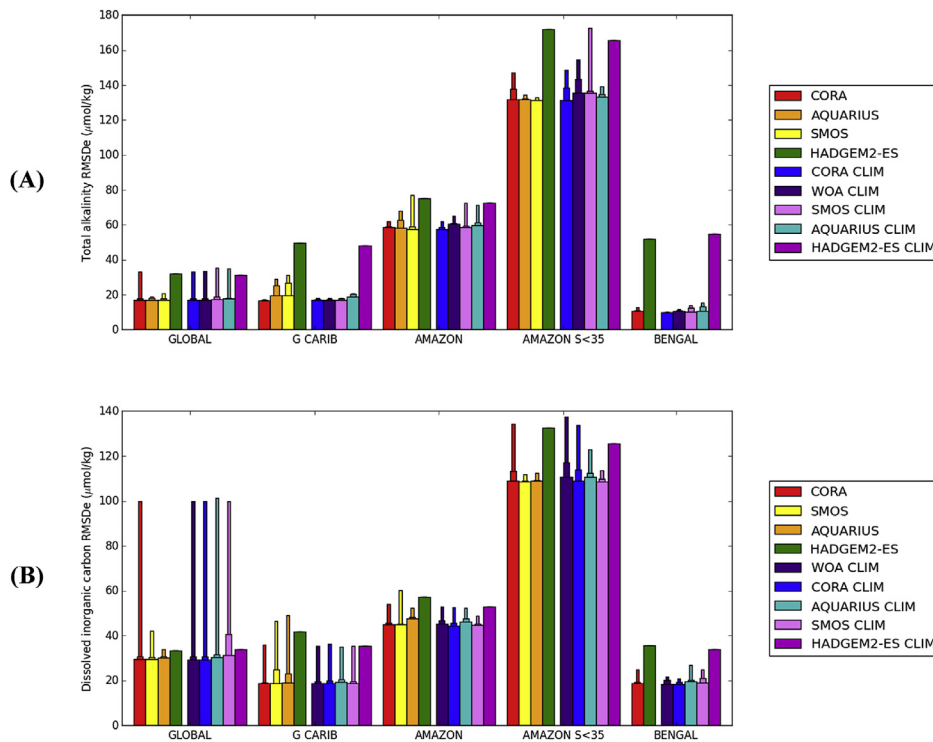


Fig. 1. Estimated regional weighted RMSD (RMSDe) for each SSS source. Data are grouped by region, then by whether the input data are climatological (left group) or monthly (right group), then by SSS source. All regional outputs using a given SSS source are considered, and the wide bar shows the lowest RMSDe of these, the half-width bar shows the median RMSDe and the thin bar shows the highest RMSDe. SSS sources in each group are shown in order of global lowest RMSDe. (A) AT results; (B) CT results.

The published algorithm uncertainties (as stated in the corresponding reference) for each algorithm were propagated through to the algorithm outputs. Following standard propagation methods (Taylor, 1997), *in situ* and algorithm uncertainties were combined assuming that they were uncorrelated (a sum of squares analysis), allowing weighted statistics to be calculated, with each data point weighted by the inverse of the sum of squared uncertainties.

2.3.2. Evaluating output accuracy

Output mean (\bar{x}_m), standard deviation (σ_m) and *in situ* carbonate data mean (\bar{x}_d) and standard deviation (σ_d) were calculated for each assessment, as well as root-mean-square-difference (RMSD), mean absolute difference (MAD), bias and point-to-point correlation (R) between output and the evaluation (GLODAPv2) *in situ* data. As a check, each of these statistics is presented both weighted and unweighted. Unweighted and weighted RMSD values were usually within about 10%, except in the case of global A_T using the TS13 algorithm, which includes regions with very different algorithm errors. Weighted statistics are used hereafter.

A potential problem with comparing outputs in this way is that different outputs overlap with different evaluation *in situ* data. Consider the plausible situation in which all outputs perform poorly in coastal waters. All else being equal, an output that is not evaluated using coastal *in situ* data will produce better statistics than one that is. Therefore, to compare like with like, in each region we considered outputs in pairs, for a given pair calculating RMSD for each of the two outputs using only *in situ* evaluation matchups shared by both outputs. Each output is given a ‘score’ of $\text{RMSD} / \text{RMSD}_{\min}$, 1 for the lower RMSD and ≥ 1 for the other. This is repeated for all possible pairs, then each output is given a ‘final score’ equal to the mean of all of its scores. To convert this to an estimate of RMSD, we chose a representative output as that with the lowest value of (weighted final score / number of matchups), i.e. the output with the best combination of performance and coverage. The weighted RMSD of this output (RMSD_{rep}) was left unchanged and all other output weighted RMSDs in the region were set to $\text{RMSD}_{\text{rep}} \times \text{final score} / (\text{final score})_{\text{rep}}$, where $(\text{final score})_{\text{rep}}$ is the final score of the representative output; this measure is henceforth

referred to as RMSDe. Output results can be compared directly within a region, but comparison of output RMSDe between regions or carbonate parameters should be treated with caution. The above calculations could equally be done using MAD in place of RMSD, though we have not done this here.

2.3.3. Evaluating optimal combinations of output elements and importances

To calculate the relative importance of different combinations of output elements (algorithms and/or data inputs) to the output comparison results, we calculated the best RMSDe when a given combination is excluded from all outputs, and divided it by the overall best RMSDe to give an RMSDe ratio. For example, the most effective single exclusion, with an RMSDe ratio of 1.022 (i.e. a 2.2% difference), is A_T using climatological CORA SSS in the Bay of Bengal. The best 13 A_T outputs in the Bay of Bengal all use climatological CORA SSS. Conversely, the best output also uses monthly CCI SST but the second best uses WOA SST, so excluding monthly CCI SST has much less effect. Excluding WOA SST has no effect, since the best output is still the one using monthly CCI SST. Having excluded climatological CORA SSS, the next 14 best A_T outputs all use the TS13 algorithm, so excluding climatological CORA SSS and TS13 has the largest effect among pairs of exclusions in this region. All possible combinations of exclusions were considered, ranked in order of number of elements excluded, then by RMSDe ratio.

The resulting comprehensive list is rather hard to read and interpret. To simplify, we created subsets of exclusions objectively considered as most significant. Criteria used were that the RMSDe ratio was greater than 1.01, the exclusions were either all SSS and/or SST inputs or all algorithms, and RMSDe ratio exceeded that of a subset of exclusions by $> 0.1\%$. For example, excluding TS13 and SMOS SSS would not qualify, and excluding SMOS and Aquarius SSS would only qualify if its RMSDe ratio were greater than excluding only SMOS and only Aquarius by $> 0.1\%$.

2.3.4. Comparing between carbonate parameters

To compare between carbonate parameters in each region, we only considered *in situ* evaluation data points where both A_T and C_T values

Table 4
Coverage, RMSDe and bias of the lowest RMSDe output for each SSS source in each region and carbonate parameter. Note that coverage is compared to all possible matchups, so recent SSS sources such as satellites have relatively low coverage.

SSS Input	Coverage (%)	RMSDe (μmol kg-1)	BIAS (μmol kg-1)
GLOBAL AT (N = 6019)			
In situ SD for comparison		81	
SSS_CORA	88	17	0
SSS_AQUARIUS	4	17	3
SSS_SMOS	6	17	-5
HG2	100	32	-17
SSS_CORA_CLIM	96	17	-2
SSS_WOA_CLIM	96	17	0
SSS_SMOS_CLIM	94	18	1
SSS_AQUARIUS_CLIM	93	18	-5
HG2_CLIM	100	31	-16
G CARIB AT (N = 55)			
In situ SD for comparison		13	
SSS_CORA	96	17	3
SSS_AQUARIUS	13	19	-4
SSS_SMOS	13	20	-4
HG2	100	50	50
SSS_CORA_CLIM	100	17	-4
SSS_WOA_CLIM	100	17	3
SSS_SMOS_CLIM	100	17	3
SSS_AQUARIUS_CLIM	100	19	2
HG2_CLIM	100	48	50
AMAZON AT (N = 108)			
In situ SD for comparison		68	
SSS_SMOS	31	58	1
SSS_AQUARIUS	12	58	17
SSS_CORA	78	59	10
HG2	100	75	43
SSS_CORA_CLIM	100	57	-1
SSS_SMOS_CLIM	100	59	-2
SSS_AQUARIUS_CLIM	100	60	1
SSS_WOA_CLIM	100	60	-6
HG2_CLIM	100	73	41
AMAZON S < 35 AT (N = 15)			
In situ SD for comparison		115	
SSS_SMOS	20	132	124
SSS_CORA	20	132	125
SSS_AQUARIUS	87	132	26
HG2	100	172	128
SSS_CORA_CLIM	100	132	25
SSS_AQUARIUS_CLIM	100	133	-19
SSS_WOA_CLIM	100	135	24
SSS_SMOS_CLIM	100	136	20
HG2_CLIM	100	166	121
BENGAL AT (N = 23)			
In situ SD for comparison		16	
SSS_CORA	96	11	-3
HG2	100	52	77
SSS_CORA_CLIM	100	10	-3
SSS_SMOS_CLIM	100	10	3
SSS_WOA_CLIM	100	11	5
SSS_AQUARIUS_CLIM	100	11	-2
HG2_CLIM	100	55	83
GLOBAL CT (N = 6689)			
In situ SD for comparison		69	
SSS_CORA	90	30	-9
SSS_SMOS	6	30	-13
SSS_AQUARIUS	3	30	23
HG2	100	33	-13
SSS_WOA_CLIM	99	29	-8
SSS_CORA_CLIM	99	29	-8
SSS_AQUARIUS_CLIM	96	30	21
SSS_SMOS_CLIM	97	31	22
HG2_CLIM	100	34	-17
G CARIB CT (N = 53)			
In situ SD for comparison		18	
SSS_CORA	96	19	14
SSS_SMOS	13	19	3
SSS_AQUARIUS	13	19	4
HG2	100	42	52

Table 4 (continued)

SSS Input	Coverage (%)	RMSDe (μmol kg-1)	BIAS (μmol kg-1)
SSS_WOA_CLIM	100	19	9
SSS_CORA_CLIM	100	19	10
SSS_SMOS_CLIM	100	19	10
SSS_AQUARIUS_CLIM	100	19	8
HG2_CLIM	100	36	45
AMAZON CT (N = 155)			
In situ SD for comparison		53	
SSS_CORA	85	45	3
SSS_SMOS	21	45	3
SSS_AQUARIUS	8	48	0
HG2	100	57	33
SSS_CORA_CLIM	100	45	0
SSS_SMOS_CLIM	100	45	0
SSS_WOA_CLIM	100	45	-2
SSS_AQUARIUS_CLIM	100	46	-1
HG2_CLIM	100	53	30
AMAZON S < 35 CT (N = 17)			
In situ SD for comparison		96	
SSS_SMOS	18	109	100
SSS_AQUARIUS	18	109	108
SSS_CORA	94	109	45
HG2	100	132	118
SSS_SMOS_CLIM	100	109	3
SSS_CORA_CLIM	100	109	44
SSS_AQUARIUS_CLIM	100	111	21
SSS_WOA_CLIM	100	111	45
HG2_CLIM	100	125	108
BENGAL CT (N = 24)			
In situ SD for comparison		10	
SSS_CORA	96	19	16
HG2	100	36	51
SSS_CORA_CLIM	100	18	-12
SSS_WOA_CLIM	100	18	-11
SSS_SMOS_CLIM	100	19	-14
SSS_AQUARIUS_CLIM	100	20	-17
HG2_CLIM	100	34	48

existed. For each data point and parameter, all outputs producing valid output were considered and the one with the best regional final score was chosen, noting the output-*in situ* difference for this output. The regional RMSD of each parameter was then calculated from the differences at all data points in the region.

3. Results

Results are summarized in Fig. 1A and B, showing RMSDe for A_T and C_T , Table 4, showing statistics of the lowest-RMSDe output for each SSS source plus HG2 output in each region, and Table 5, showing selected importances. Fig. 2 to 4 contain plots of output versus evaluation (GLODAPv2) *in situ* A_T , C_T and SSS data, with points with depth < 500 m and > 300 km from the coast labeled. Alternative versions of Fig. 1A and B for differing masks are shown in Fig. S1. Supporting data (Land et al., 2019) consist of three data collections corresponding to all data, minimum depth 500 m, and minimum depth 500 m plus minimum distance to coast 300 km; matchup data, output statistics, details of output score calculations, spatial data results, importances of exclusions and the comparisons between carbonate parameters (also included in Supplementary Information) are included.

Generally there is little to choose between the SSS sources (re-analysed *in situ* or satellite) apart from HG2, which performs less well in all regions, or between monthly and climatological SSS sources. The main differences in performance are between algorithms and between regions, but there is no clearly superior algorithm.

3.1. Total alkalinity (A_T)

See Table 4 for detailed results. Globally, the best RMSDe values of

Table 5

Selected importances of exclusions for each carbonate parameter and region. A source of SSS or SST can be monthly (M), climatological (C) or all (no prefix). Importances are the percentage increase in RMSDe as a result of excluding all the listed inputs or algorithms. Only exclusions mentioned in the text are listed here, more complete lists can be found in (Land et al., 2019).

Exclusions	Importance (%)	Notes
(GLOBAL A_T)		
TS13,L06,S13g	3.1	Only leaves S13,HG2
TS13,L06,S13g,S13	85	Only leaves HG2
CORA,M SMOS,M Aquarius,WOA SSS	3.0	Only leaves C SMOS,C Aquarius
CORA,SMOS,M Aquarius,WOA SSS	4.1	Only leaves C Aquarius
(G CARIB A_T)		
CORA,WOA,C SMOS SSS	13	Only leaves M SMOS,Aquarius
TS13,L06,S13g,Cai10	2.9	Only leaves S13,HG2
TS13,L06,S13g,Cai10,S13	286	Only leaves HG2
CORA,WOA,C Aquarius,C SMOS SSS	16	Only leaves M SMOS,M Aquarius
CORA,WOA,Aquarius,C SMOS SSS	18	Only leaves M SMOS
(AMAZON A_T)		
TS13,L06,S13,S13g	2.6	
TS13,L06,S13,S13g,Cai10	4.4	Only leaves Lefevre10,HG2
SMOS,CORA,M Aquarius SSS	4.0	Only leaves C Aquarius,WOA SSS
TS13,L06,S13,S13g,Cai10,Lefevre10	26	Only leaves HG2
SMOS,CORA,Aquarius SSS	5.1	Only leaves WOA SSS
(AMAZON $S < 35 A_T$)		
M SMOS,M Aquarius SSS,M CCI SST	2.5	All monthly satellite data
M SMOS,Aquarius SSS,M CCI SST	3.2	
SMOS,Aquarius SSS,M CCI SST	4.6	
M SMOS,Aquarius,CORA SSS	2.9	
TS13,L06,S13,S13g,Cai10,Lefevre10	26	Only leaves HG2
(BENGAL A_T)		
C CORA SSS	2.2	
C CORA,C SMOS SSS	5.1	
C CORA,C SMOS,WOA SSS	6.4	Only leaves M CORA,C Aquarius
TS13,L06,S13	3.7	Only leaves S13g,HG2
TS13,L06,S13,S13g	517	Only leaves HG2
CORA,C SMOS,WOA SSS	8.1	Only leaves C Aquarius
(GLOBAL C_T)		
L00	3.6	
L00,S13g	5.3	
L00,S13g,S13	14	Only leaves HG2
CORA,WOA,M SMOS SSS	3.6	
CORA,WOA,M SMOS,M Aquarius SSS	4.4	Only leaves C SMOS,C Aquarius
CORA,WOA,Aquarius,M SMOS SSS	7.7	Only leaves C SMOS
(G CARIB C_T)		
L00,S13	73	Only leaves S13g and HG2
L00,S13,S13g	90	Only leaves HG2
SMOS,CORA,WOA,M Aquarius SSS	3.9	Only leaves C Aquarius
(AMAZON C_T)		
L00,S13,Bonou16,Lefevre10	2.1	Only leaves S13g and HG2
L00,S13,Bonou16,Lefevre10,S13g	19	Only leaves HG2
SMOS,CORA,WOA SSS	3.6	Only leaves Aquarius
SMOS,CORA,C Aquarius,WOA SSS	7.0	Only leaves M Aquarius
(AMAZON $S < 35 C_T$)		
L00,S13,Bonou16,Lefevre10	2.2	Only leaves S13g and HG2
L00,S13,Bonou16,Lefevre10,S13g	15	Only leaves HG2
SMOS,Aquarius SSS,M CCI SST	2.6	Only leaves CORA,WOA SSS
SMOS,Aquarius,CORA SSS,M CCI SST	4.9	Only leaves WOA SSS
(BENGAL C_T)		
S13	2.1	
S13,S13g	9.9	

Table 5 (continued)

Exclusions	Importance (%)	Notes
C CORA,WOA SSS	2.1	
L00,S13,S13g	83	Only leaves HG2
CORA,WOA SSS	3.6	
CORA,C SMOS,WOA SSS	5.9	

about $17 \mu\text{mol kg}^{-1}$ are substantially lower than the SD of the global coverage *in situ* data used for the evaluation ($81 \mu\text{mol kg}^{-1}$), and in the Amazon and Bay of Bengal they are slightly lower (RMSDe of 55 compared to a SD of 68, and RMSDe of 11 compared to a SD of $16 \mu\text{mol kg}^{-1}$, respectively), but in the Greater Caribbean and low-salinity Amazon the RMSDe are higher than the SD, meaning that none of the tested combinations of algorithms and inputs is accurate enough to distinguish natural variations in A_T in these latter two regions.

3.1.1. A_T algorithm and input importances

See Table 5 for details. Globally, S13 performs slightly less well (higher RMSDe) than other algorithms, as do climatological satellite inputs. In the Greater Caribbean, monthly SMOS and Aquarius and climatological Aquarius SSS perform significantly less well. In the Amazon, the Lefevre et al. (2010) algorithm and climatological Aquarius and WOA SSS perform less well. In the low-salinity Amazon, monthly SMOS and Aquarius and monthly CCI SST perform best. In the Bay of Bengal, climatological CORA SSS performs best and climatological Aquarius performs significantly less well.

3.1.2. A_T summary

For all case study regions and with respect to these empirical outputs, satellite SSS can reproduce *in situ* measured A_T from the GLODAPv2 evaluation dataset with performance (RMSDe) comparable to, or better than, the re-analysed *in situ* data derived inputs for SSS, and the satellite based A_T is always better than HG2 A_T estimates. Globally HG2 performance is about 85% worse than the best SSS driven outputs, but this reduces to 15–20% in the Amazon plume. Monthly Aquarius and SMOS observations provide a credible solution to monitoring synoptic scale global and regional A_T , though in some challenging regions (Greater Caribbean and low-salinity Amazon plume) none of the tested methods are sufficiently accurate to resolve natural variability.

RMSDe in the Amazon plume is higher than the global RMSDe, reflecting the larger regional standard deviation in the *in situ* data due to the large gradients around the river flow, and RMSDe in the Amazon with $SSS < 35$ is higher than in the wider Amazon, but the relative performance of SSS inputs is similar.

Excluding the Amazon plume and HG2, the best outputs have bias less than $5 \mu\text{mol kg}^{-1}$, or 0.2% of the global mean A_T (of $2450 \mu\text{mol kg}^{-1}$) which is similar to the estimated evaluation dataset *in situ* nominal uncertainty of 0.5% (Bockmon et al., 2015) and the inter-annual variability of A_T observed at oceanic sites such as at the Hawaiian Ocean Time-series station (HOT; $\pm 6 \mu\text{mol kg}^{-1}$) (Brix et al., 2004), but lower than the seasonal variability observed at oceanic sites (20 to $30 \mu\text{mol kg}^{-1}$ at both the Bermuda Atlantic Time-series Study (BATS) (Bates et al., 2012) and the European time series station (ESTOC) (Santana-Casiano et al., 2007). This seasonal variability at BATS and ESTOC is also greater than the best global RMSDe of $17 \mu\text{mol kg}^{-1}$. In the Amazon plume, of the monthly SSS sources only SMOS has low bias ($2 \mu\text{mol kg}^{-1}$), and in the low-salinity Amazon plume, all SSS sources have bias greater than $19 \mu\text{mol kg}^{-1}$. These results highlight that these methods (of using satellite observations or re-analysed *in situ* dataset as input to empirical algorithms) can obtain measures of A_T that are not significantly biased relative to the evaluation *in situ* measurements, except in regions of strong spatiotemporal variability. It also shows that these methods are capable of distinguishing the seasonal variability at long-term time series sites, though

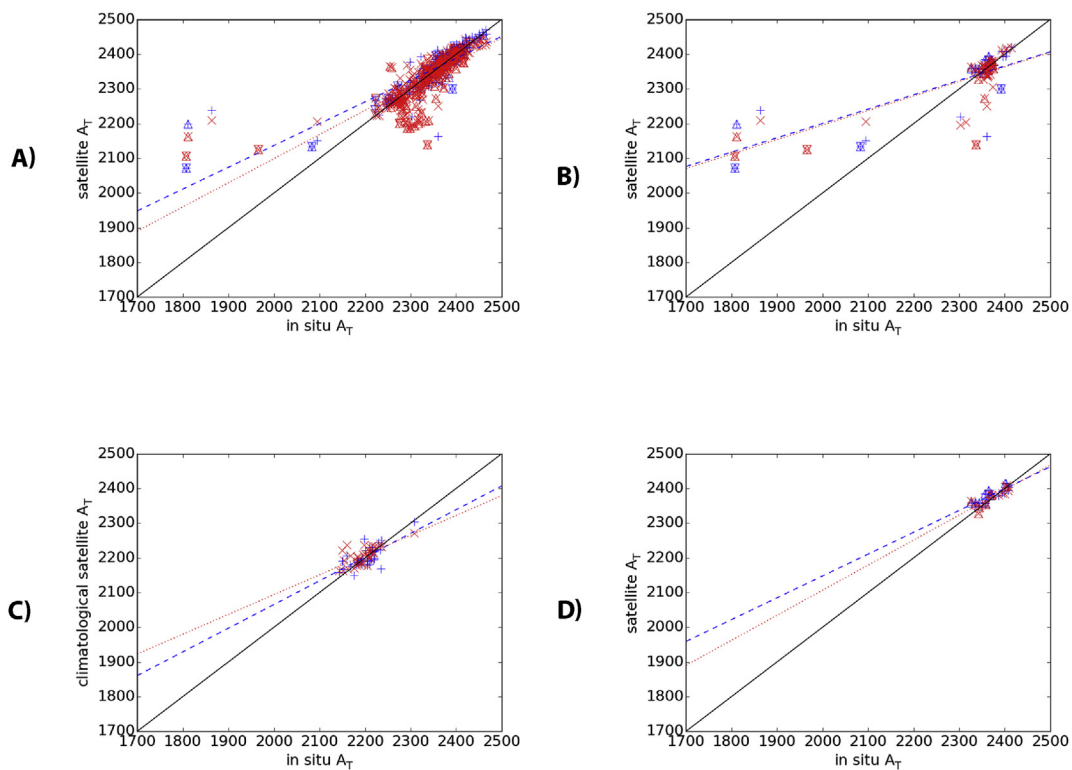


Fig. 2. Comparison of AT estimated using monthly satellite SSS with *in situ* measured AT. (A) global; (B) Amazon plume; (C) Bay of Bengal using climatological satellite SSS; (D) Greater Caribbean. The algorithm is (Takahashi et al., 2013) with climatological WOA nitrate. Red crosses use SMOS SSS, blue pluses use Aquarius. Points with down-pointing triangles have depth less than 500 m, those with up-pointing triangles are less than 300 km from the nearest coast. Regressions use all data.

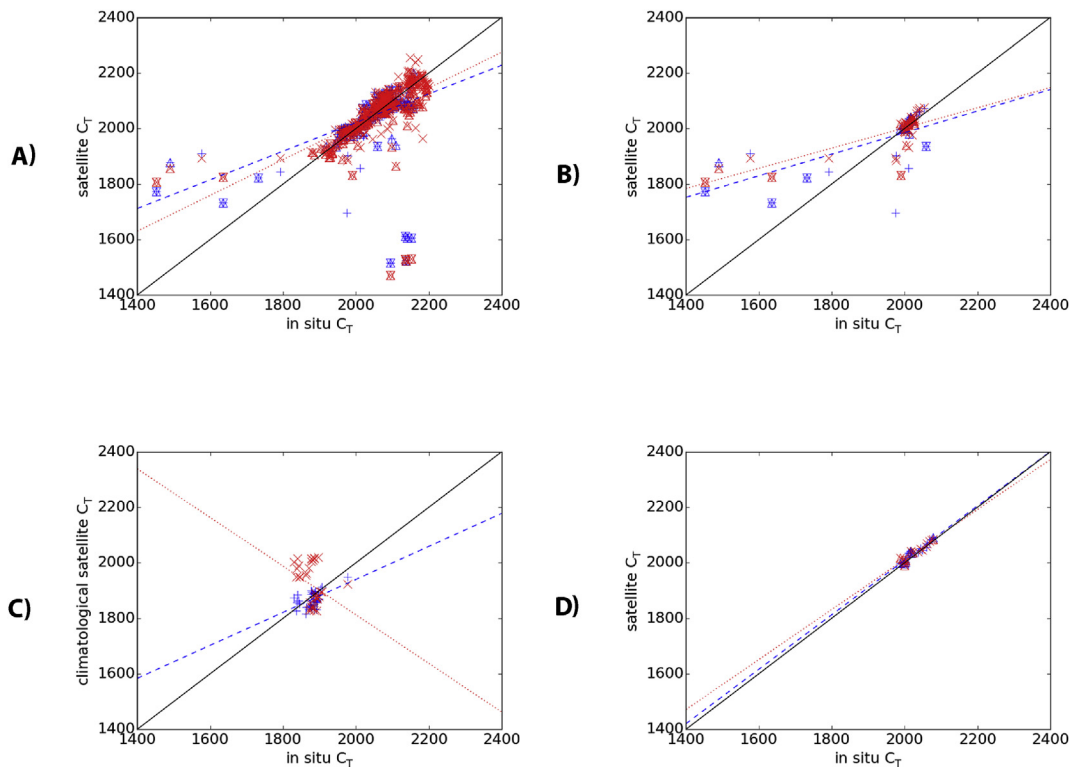


Fig. 3. Comparison of CT estimated using monthly satellite SSS with *in situ* measured CT. (A) global; (B) Amazon plume; (C) Bay of Bengal using climatological satellite SSS; (D) Greater Caribbean. The algorithm is (Lee et al., 2000) with climatological WOA SST and nitrate. Red crosses use SMOS SSS, blue pluses use Aquarius. Points with down-pointing triangles have depth less than 500 m, those with up-pointing triangles are less than 300 km from the nearest coast. Regressions use all data.

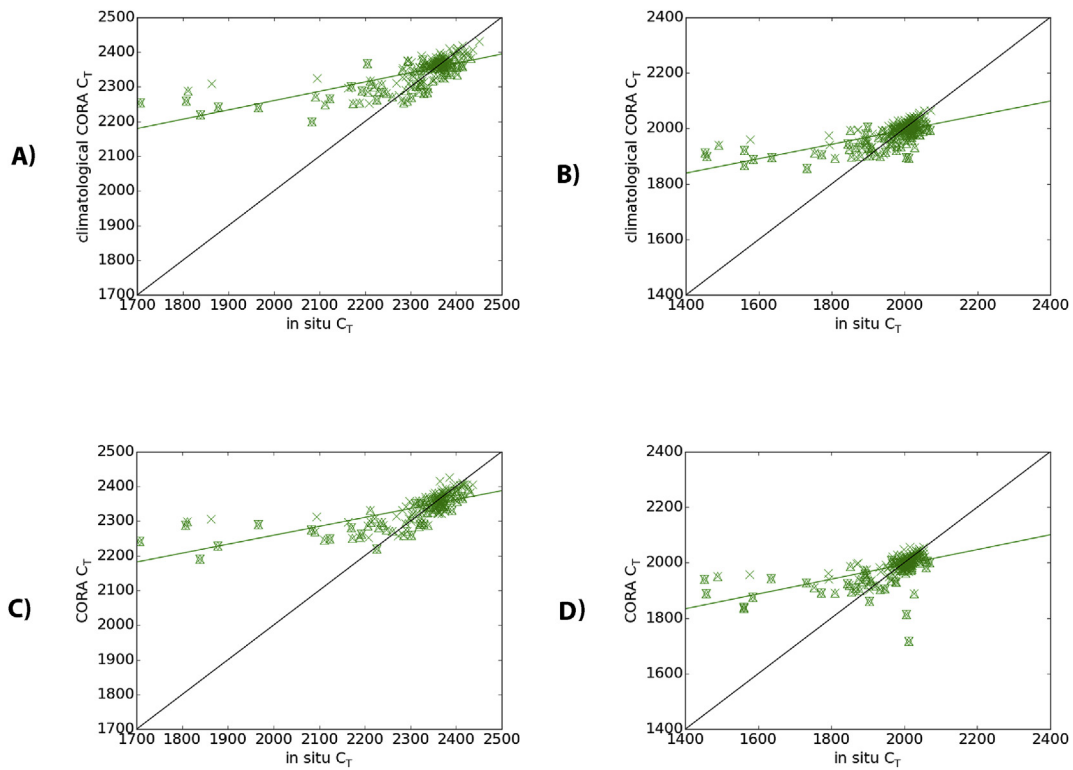


Fig. 4. Comparison of AT and CT estimated from CORA (interpolated *in situ*) SSS with *in situ* measured values in the Amazon plume. (A) AT comparison using climatological CORA SSS; (B) CT comparison using climatological CORA SSS; (C) AT comparison using monthly CORA SSS; (D) CT comparison using monthly CORA SSS. The AT algorithm is (Takahashi and Sutherland, 2013) with climatological WOA nitrate, and the CT algorithm is (Lee et al., 2000) with climatological CORA SST and climatological WOA nitrate. Points with down-pointing triangles have depth less than 500 m, those with up-pointing triangles are less than 300 km from the nearest coast. Regressions use all data.

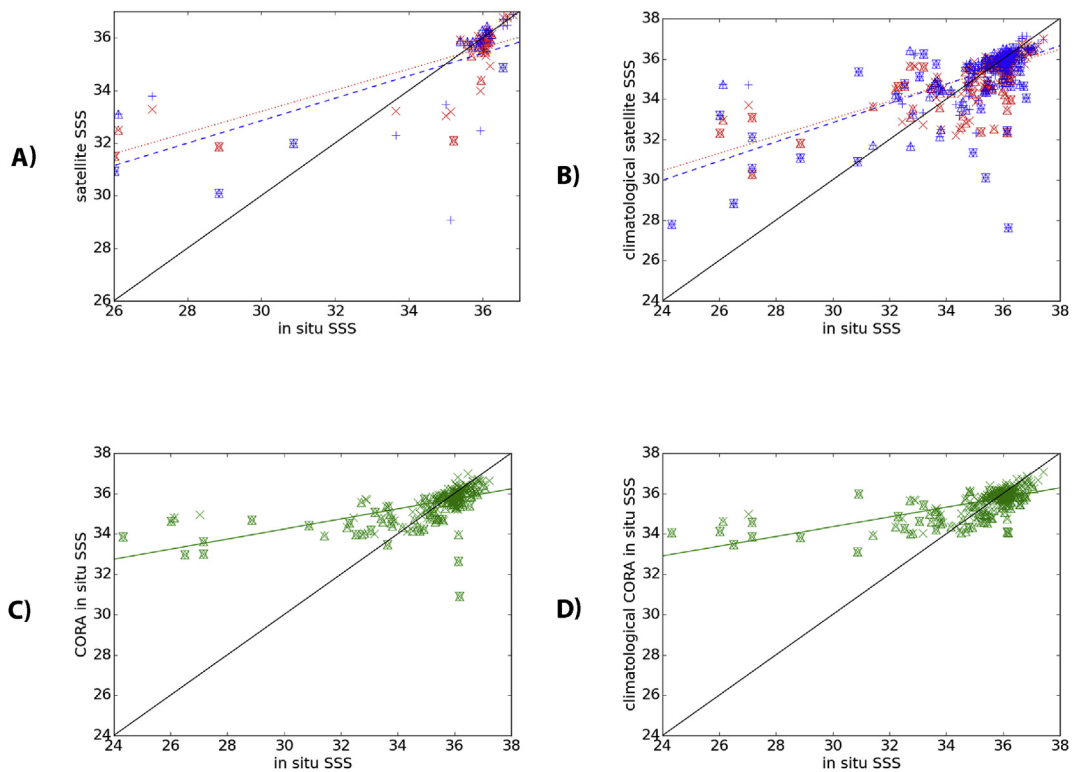


Fig. 5. Comparison of satellite and CORA SSS with *in situ* measured SSS in the Amazon plume. (A) monthly SMOS (red crosses) and Aquarius (blue pluses); (B) climatological SMOS and Aquarius; (C) monthly CORA; (D) climatological CORA. Points with down-pointing triangles have depth less than 500 m, those with up-pointing triangles are less than 300 km from the nearest coast. Regressions use all data.

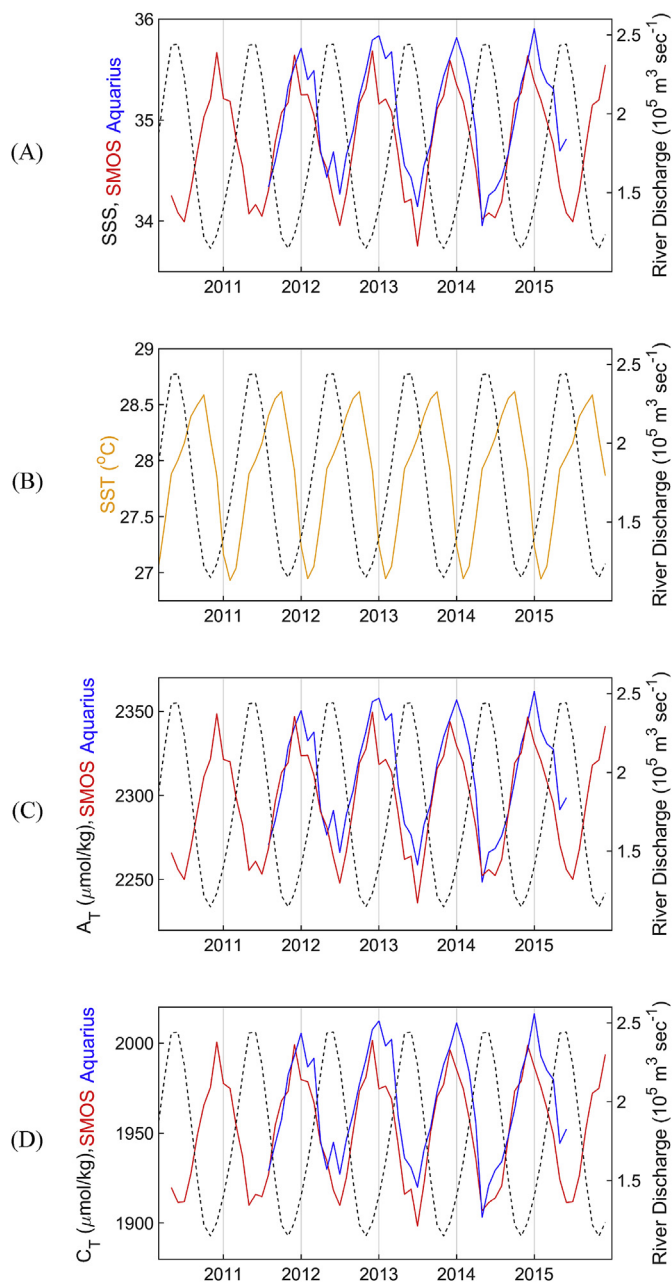


Fig. 6. Time series of Amazon plume discharge and averaged satellite observations between 2010 and 2016. Monthly observations were average over the area 0° – 15° N, 45° – 62° W. Dashed black lines are climatological discharge at the Obidos gauge, red use SMOS SSS and blue use Aquarius SSS. In months containing both SMOS and Aquarius data, only cells with valid data in both are used. (A) monthly SMOS and Aquarius SSS; (B) climatological CORA (orange) SST; (C) AT using the TS13 algorithm and WOA nitrate, with monthly SMOS and Aquarius SSS; (D) CT using the L00 algorithm, CORA SST climatology and WOA nitrate, with monthly SMOS and Aquarius SSS.

not the interannual variability at HOT.

3.2. Total dissolved inorganic carbon (C_T)

See Table 4 for detailed results. Globally, the best RMSDe values of 29 – $30 \mu\text{mol kg}^{-1}$ are considerably higher than the equivalent global A_T RMSDe values, but still substantially lower than the SD of the global *in situ* evaluation dataset ($69 \mu\text{mol kg}^{-1}$), and in the Amazon and Greater Caribbean they are similar (RMSDe 45 compared to SD 53 and RMSDe 19 compared to SD $18 \mu\text{mol kg}^{-1}$, respectively), but in the low-salinity

Amazon and Bay of Bengal they are higher, meaning that no combination of algorithms and inputs is accurate enough to distinguish natural variations in C_T in these latter two regions.

3.2.1. C_T algorithm and input importances

See Table 5 for details. Globally, L00 and S13g perform better (lower RMSDe) than other algorithms, as do CORA, WOA and monthly SMOS SSS inputs. In the Greater Caribbean, the S13g algorithm performs very poorly and climatological Aquarius SSS performs less well than other SSS inputs. In the Amazon, the S13g algorithm and Aquarius SSS perform less well. In the low-salinity Amazon, the S13g algorithm performs less well, while SMOS, Aquarius and monthly CCI SST perform best. In the Bay of Bengal, the S13 and S13g algorithms perform considerably better than other algorithms and CORA and WOA SSS perform better than other SSS sources.

3.2.2. C_T summary

Similar to A_T , satellite inputs for SSS can reproduce the C_T data (from the GLODAPv2 evaluation dataset) with similar ability, and sometimes better than using re-analysed or climatology *in situ* derived SSS inputs, except for Aquarius in the Amazon plume (Fig. 1B), and always better than HG2 C_T estimates. Global HG2 performance is only about 14% worse than the best SSS driven outputs, but this increases to over 80% in the Bay of Bengal and Greater Caribbean. As with A_T , monthly SMOS and Aquarius observations provide a credible solution to monitoring synoptic scale global and in some cases regional C_T . Best RMSDe values are higher for C_T than A_T globally and in the Greater Caribbean and Bay of Bengal, but lower in both Amazon plume regions. Again, in some challenging regions (low-salinity Amazon plume and Bay of Bengal), none of the tested methods are sufficiently accurate to reproduce natural variations.

Bias in the C_T outputs is generally greater and more variable than that in the A_T outputs, except in the Amazon plume where non-HG2 monthly and climatological bias is uniformly less than $3 \mu\text{mol kg}^{-1}$. The smallest bias among the best global monthly outputs is monthly CORA with $-9 \mu\text{mol kg}^{-1}$, in the Greater Caribbean monthly SMOS and Aquarius have bias of 3 and $4 \mu\text{mol kg}^{-1}$ respectively, monthly outputs in the low-salinity Amazon are all strongly biased, the smallest being CORA with $45 \mu\text{mol kg}^{-1}$, and in the Bay of Bengal monthly CORA has bias of $16 \mu\text{mol kg}^{-1}$ while climatological datasets (WOA, CORA, SMOS) have lower bias (-11 , -12 , $-14 \mu\text{mol kg}^{-1}$ respectively). For comparison, the *in situ* nominal uncertainty of 0.5% (Bockmon et al., 2015) at the global average C_T of $1900 \mu\text{mol kg}^{-1}$ would be $9.5 \mu\text{mol kg}^{-1}$, the inter-annual variability of nC_T is $\pm 4 \mu\text{mol kg}^{-1}$ at HOT and $\pm 8 \mu\text{mol kg}^{-1}$ at ESTOC (Brix et al., 2004, Santana-Casiano et al., 2007), while the seasonal amplitude of nC_T at HOT is $15 \mu\text{mol kg}^{-1}$ (Brix et al., 2004) and those of C_T at ESTOC and BATS are 20 – 30 and 40 – $50 \mu\text{mol kg}^{-1}$, respectively (Santana-Casiano et al., 2007; Bates et al., 2012). The biases in these outputs are also comparable to the systematic biases found by Lee et al. (2000) when comparing algorithm derived nC_T to nC_T calculated from A_T and $p\text{CO}_2$ data (-3 to $+15 \mu\text{mol kg}^{-1}$). Thus, these results highlight that some of the outputs evaluated can obtain measures of C_T that are not significantly biased relative to the *in situ* evaluation measurements, though overall uncertainties may be high relative to the variability at these long-term monitoring sites.

3.3. A_T and C_T algorithm biases

In the Amazon Plume, the best output was strongly correlated with the evaluation *in situ* A_T or C_T , but with a slope significantly different from 1 (Figs. 2B and 3B). Replacing monthly satellite SSS with monthly or climatological CORA SSS (re-analysed and interpolated *in situ*) produces similar biases (Fig. 4), suggesting that the cause of the bias is not specific to satellite SSS or monthly data.

A possible explanation of this bias would be that the algorithm is not

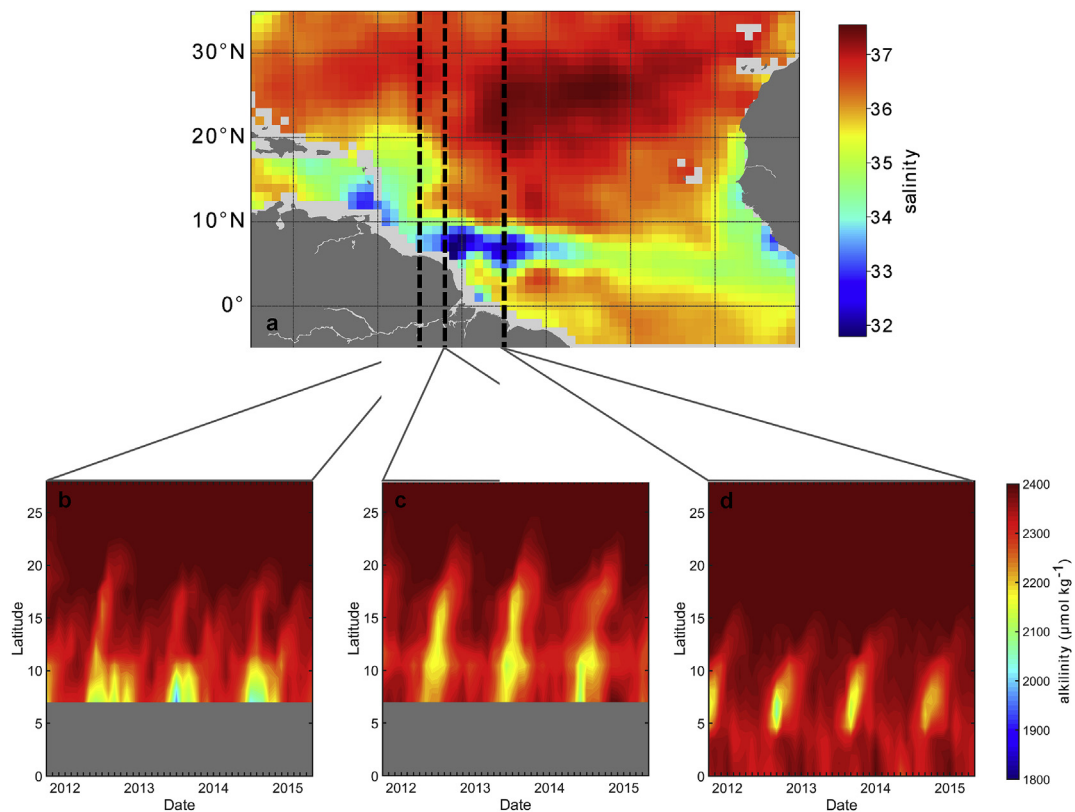


Fig. 7. Aquarius derived synoptic scale observations of AT in $\mu\text{mol kg}^{-1}$ for the Amazon Plume between August 2011 and June 2015 using the TS13 algorithm and WOA nitrate, with monthly SMOS and Aquarius SSS: (a) AT in August 2011 showing the bifurcation of the plume; (b) Hovmöller time series plot for 55°W ; (c) Hovmöller time series plot for 52°W and (d) Hovmöller time series plot for 45°W .

capturing the two endmember mixing from the river with zero salinity and some finite, but significant A_T and C_T . However, the regional algorithms for the Amazon plume implicitly include the river endmember, as they are based on measurements that include low and high salinity values, and each published algorithm finds a strongly linear relationship between salinity and A_T or C_T . Since the bias using these algorithms is similar to that using the global algorithms, we can conclude that the endmember issue is not the main reason for the bias.

Another possible explanation of the bias would be sampling of water with low SSS, A_T and C_T in regions with high spatial and temporal SSS variability, as found in the Amazon plume and particularly within the low salinity Amazon plume region. Satellite and CORA data represent an average over at best one grid cell (about 10^4 square kilometers at the equator) and one month (or the same month in a range of years in the case of climatological data), while an *in situ* measurement samples a very small volume of water and is almost instantaneous. The effect of this averaging is to remove variability that occurs on smaller spatial and temporal scales. For example, low *in situ* salinity in the Amazon plume may be caused by small eddies or filaments of river water not resolvable at the grid cell scale, or by interannual variations in the plume extent. In this situation, extreme evaluation *in situ* values will consistently be matched with outputs driven by satellite and CORA data that are closer to the large-scale and long-term mean. If the salinity distribution is strongly one-tailed, as in the Amazon plume, and the cause of anomalies is consistently unresolved by the averaged data, the *in situ* evaluation data will consistently give lower salinity than the averaged data, as observed here (Fig. 5). This issue is likely to be one cause of the large biases evident in all output results (re-analysed *in situ* and satellite input derived) for the low salinity Amazon region.

A third possible explanation for the bias arises from fundamental differences between the *in situ* measurements used to calibrate the original algorithms and the satellite salinity observations used herein as

input to the algorithms. Satellite SSS observations represent the conditions in the top 10 mm of the water (Boutin et al., 2013), whereas *in situ* SSS observations are typically sampled from ≥ 1 m below the surface. This can result in geophysical sources of variation between satellite and *in situ* salinity, which are linked to vertical salinity stratification, and these features are prevalent in regions of rain, oceanic fronts and river outflow (Boutin et al., 2013, 2016; Drucker and Riser, 2014). For example, salinity gradients created by freshwater plumes can complicate the comparison of satellite and *in situ* salinity measurements; a difference of $2\text{--}5$ pss m^{-1} has been observed across the halocline in the Amazon plume (Lentz and Limeburner, 1995). Plumes can also cause horizontal salinity gradients with spatial scales smaller than the footprint of the satellite radiometers. Typical horizontal SSS gradients for the plumes from the Amazon (Lentz and Limeburner, 1995) or Congo (Chao et al., 2015) exceed 0.2 pss km^{-1} and extend more than 250 km from the river mouth. Therefore, in the vicinity of a river plume, a spatially sparse array of *in situ* sensors can exhibit very different SSS variability from that observed by a satellite sensor, even if the measurements are all coincident. Similarly, high-frequency SSS variations (e.g. tidal effects) can be undersampled by satellite-derived SSS products due to the relatively long revisit time of the satellite (2–3 days for SMOS and 7 days for Aquarius). Accounting for the depth-related differences should increase the accuracy of the outputs, and a rigorous treatment might adapt the theory currently used to reconcile *in situ* and satellite SST (Merchant et al., 2014). We therefore recommend that the satellite SSS community consider investigating this theory for SSS.

In the absence of a rigorously tested explanation for these biases, and to demonstrate the potential gain from reducing them, we simply note that linear regression of the best output against the evaluation *in situ* A_T and C_T reduces the RMSD (actual, not estimated) in the low salinity Amazon plume region from 215 to 48 $\mu\text{mol kg}^{-1}$ (a 77%

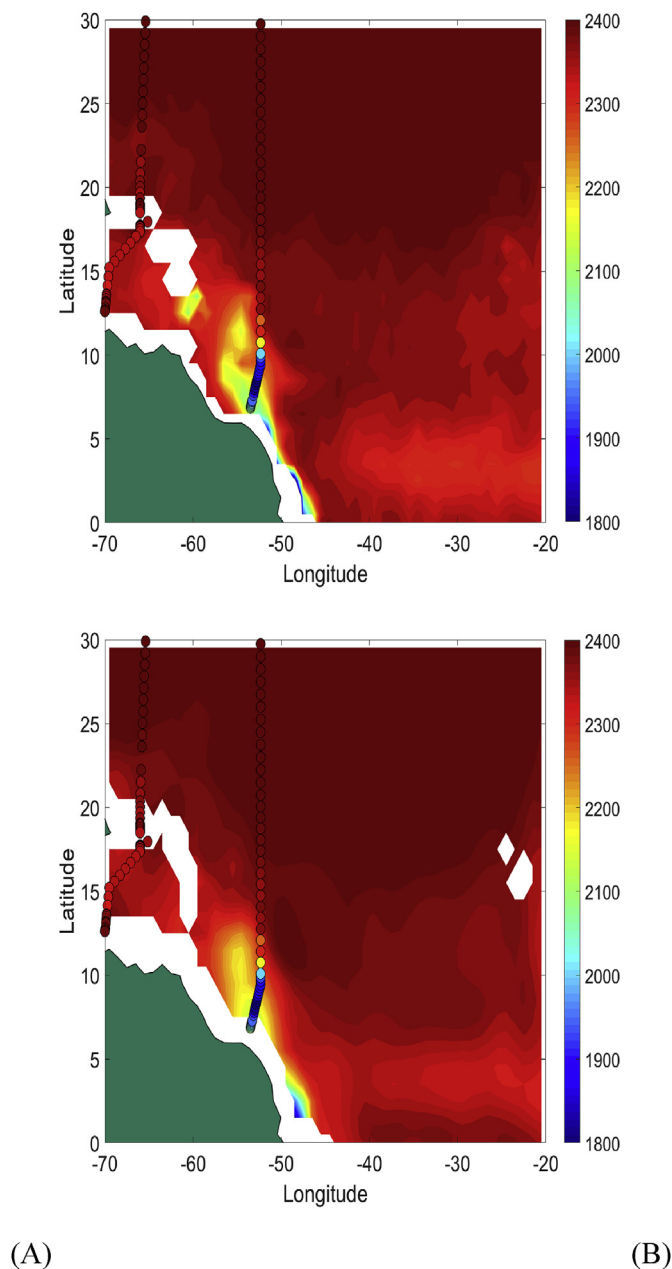


Fig. 8. Synoptic scale Aquarius (A) and SMOS (B) derived A_T in $\mu\text{mol kg}^{-1}$ for April 2012 using the TS13 algorithm and WOA nitrate, with monthly SMOS and Aquarius SSS. In situ observations collected in April and May 2012 from the GLODAPv2 dataset are overlaid as circles. The May 2012 *in situ* observations are all within the offshore region (latitude $> 20^\circ$ N).

reduction) for A_T and from 67 to $50 \mu\text{mol kg}^{-1}$ (26%) for C_T .

3.4. Comparison of A_T with C_T

Results are shown in Dataset S23, showing that in direct comparisons at each matchup position, the A_T outputs have a 42% lower RMSDe than C_T globally, 41% lower in the Bay of Bengal and 21% lower in the Caribbean, indicating that A_T outputs can generally be retrieved more successfully than C_T outputs. However, A_T has a 13% higher RMSDe than C_T in the Amazon and 9% higher in the low salinity Amazon using the same algorithms as in the global case, so this relationship is not universal.

3.5. Multi-year synoptic observations

The methods evaluated here enable the first multi-year synoptic scale observations of A_T and C_T spatial mixing and distributions. To demonstrate their application we characterise the synoptic scale, extent and influence of river-flow-dominated alkalinity mixing in the Amazon plume and western North Atlantic. The Amazon Plume exhibits a two-end-member alkalinity-salinity mixing regime, resulting in a strong linear relationship between alkalinity and salinity (Cai et al., 2010), and mixing between river water and seawater is the dominant controlling factor of the alkalinity-salinity relationship in the western North Atlantic (Jiang et al., 2014). The accuracy assessment means that we can illustrate SMOS or Aquarius observational-based C_T and A_T monitoring of the Amazon plume along with a calculated estimate of the combined uncertainty in C_T and A_T (provided by the RMSDe and bias).

To simplify the interpretation we present results using the same algorithm for monthly SMOS and Aquarius, so that any differences are due solely to the SSS source. For A_T , the best output with both SMOS and Aquarius is TS13 with WOA nitrate, with RMSDe of $57.7 \mu\text{mol kg}^{-1}$ for SMOS and $58.4 \mu\text{mol kg}^{-1}$ for Aquarius. For C_T the best Aquarius outputs use different algorithms to the best SMOS outputs, and perform less well. Therefore for simplicity we present results of using SMOS and Aquarius with a single algorithm and input pairing (L00 and climatological CORA SST), with RMSDe of $45.0 \mu\text{mol kg}^{-1}$ for SMOS and $52.2 \mu\text{mol kg}^{-1}$ for Aquarius. We calculated A_T and C_T time series for the Amazon plume using the above algorithm and input pairings, producing monthly Aquarius and SMOS derived A_T and C_T collectively covering the time period 2010 to 2016.

Fig. 6 shows the regional ($0\text{--}15^\circ\text{N}$, $45\text{--}62^\circ\text{W}$) mean SMOS and Aquarius SSS, climatological CORA SST, output A_T and output C_T , in relation to climatological Amazon discharge data from the Obidos gauge located 750 km from the ocean (Perry et al., 1996). The discharge data are only provided as an indication of variations in Amazon discharge and will not represent the total flow (Salisbury et al., 2011). In a given month with both SMOS and Aquarius data, we calculate mean SSS using only cells in which both have valid data, in order to compare like with like. If this is not done, and one dataset extends into a low salinity region not covered by the other, large spurious differences can occur, e.g. in May 2014 inconsistent masking causes the regional mean Aquarius SSS to be 1.24 units lower than SMOS SSS (results not shown), a difference that reduced to 0.07 units with consistent masking. Maximum SSS consistently occurs during December and January and minimum SSS occurs during May–July, 1–3 months after the maximum discharge in April, both of which are consistent with previous findings (Salisbury et al., 2011). As expected, A_T and C_T maxima occur in phase with the variations in SSS, and typically lag the peaks in SST by one to two months, with regional A_T each year varying between 2230 and $2370 \mu\text{mol kg}^{-1}$ and C_T varying between 1890 and $2000 \mu\text{mol kg}^{-1}$.

Fig. 7 reveals the seasonal patterns in A_T over the same period as shown in Fig. 6B in relation to the dynamics of the Amazon discharge and their interaction offshore with the along-shore North Brazilian Current, North Equatorial Counter Current and Guyana Current. The August 2011 SSS conditions are shown in Fig. 7A. Clear annual cycles and river plume features are apparent in the observed A_T , with the Amazon plume influencing A_T more than 1000 km offshore of the mouth of the Amazon (Fig. 7B–D). During June–July each year, very low A_T values reaching below $2100 \mu\text{mol kg}^{-1}$ are apparent at the mouth of the Amazon (Fig. 7D), the timing of which is consistent with the observed annual minima in SSS (Salisbury et al., 2011) (see also Fig. 6). Further west the river plume spreads out as it interacts with the along-shore currents, resulting in A_T in the region of $\sim 2150 \mu\text{mol kg}^{-1}$ up to ~ 1700 km offshore (regions of yellow up to $\sim 17^\circ\text{N}$ in Fig. 3C). The Amazon plume has been observed to bifurcate during the northern hemisphere summer months (Del Vecchio and Subramaniam, 2004), with one part of the river plume heading north-west and a second jet

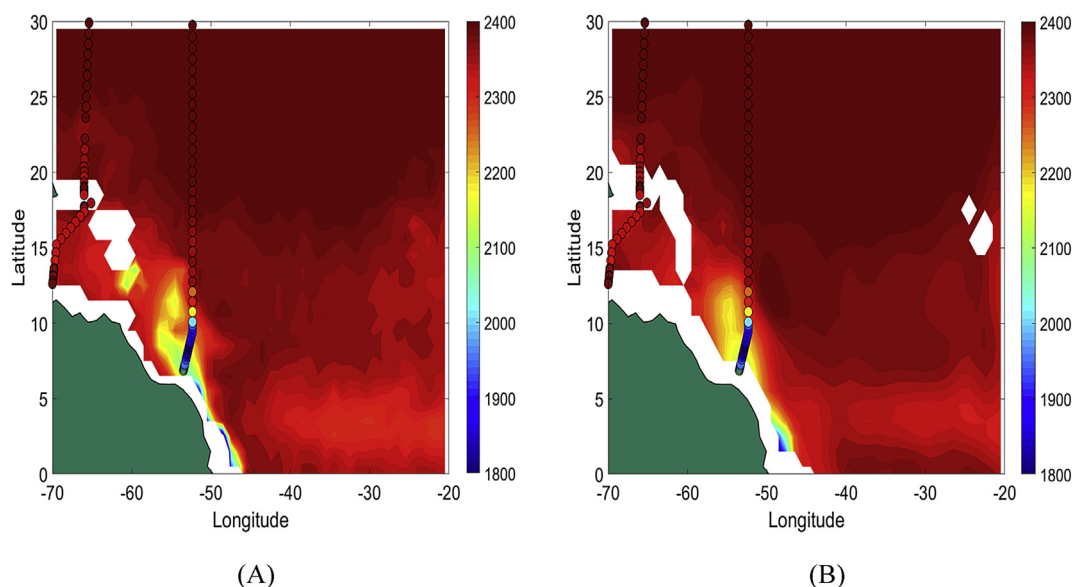


Fig. 9. Synoptic scale Aquarius (A) and SMOS (B) derived C_T in $\mu\text{mol kg}^{-1}$ for April 2012 using the L00 algorithm, CORA SST climatology and WOA nitrate, with monthly SMOS and Aquarius SSS. In situ observations collected in April and May 2012 from the GLODAPv2 dataset are overlaid as circles. The May 2012 *in situ* observations are all within the offshore region (latitude $> 20^\circ$ N).

Table 6

Testing the sensitivity of the output uncertainties to the satellite remote sensing input data uncertainties using all global AT algorithms (TS13, Lee06, Lee00, S13 and S13g) with climatological WOA inputs perturbed by exemplar uncertainties from the literature (for SST, Merchant et al., (2014) gives $\pm 0.15^\circ\text{C}$; for SSS, Boutin et al., (2018) gives ± 0.2). The output uncertainties are given as a percentage of the unperturbed value and the quoted values are the maximum open-ocean uncertainties calculated for all data within latitudes $< \pm 60^\circ$.

Algorithm	Uncertainty in AT due to SSS (%)	Uncertainty in AT due to SST (%)
TS13	$< \pm 0.8$	N/A
Lee06	$< \pm 0.7$	$< \pm 0.2$
Lee00	$< \pm 0.9$	$< \pm 0.2$
S13	$< \pm 0.6$	$< \pm 0.1$
S13g	$< \pm 0.6$	$< \pm 0.1$

retroflected to the east (Salisbury et al., 2011). This bifurcation is apparent each year around August (Fig. 7A–D), with an isolated feature of A_T around $2000\text{--}2100 \mu\text{mol kg}^{-1}$ appearing $500\text{--}1000$ km offshore and to the east of the river mouth, although this feature was less pronounced during 2014 (regions of yellow between $5\text{--}10^\circ\text{N}$ in Fig. 7D).

Fig. 8 shows Aquarius and SMOS monthly A_T for April 2012 overlaid with 100 *in situ* A_T observations from the GLODAPv2 dataset (Olsen et al., 2016) collected at 3 m nominal depth during 13 consecutive days in April and May 2012, and Fig. 9 shows the equivalent plot for C_T . Despite the different temporal resolutions, the change in magnitude of the observations (the gradient) between the open ocean data and those close to, and within the river plume, are generally comparable to the synoptic scale observations. The high monthly temporal variations along the $\sim 52^\circ\text{W}$ latitudinal transect are illustrated in Fig. 7D. The differences between *in situ* and synoptic scale observations are discussed in section 3.3. This comparison highlights the power of the synoptic scale observations, allowing the *in situ* observations to be placed within their wider spatial and temporal context. It also highlights how the synoptic observations characterise the distributions and mixing at the very surface of the water column and how these can be different from that observed *in situ* (at a nominal depth of 3 m), particularly in regions of strong river plume influence. Figs. 8 and 9 could suggest that lower values of A_T and C_T are found below the surface in the coastal region, whereas offshore the salinity, A_T and C_T are vertically well mixed. A combination of *in situ* and synoptic scale observations could be used to

understand the near-surface vertical profile of A_T .

4. Discussion

4.1. Bay of Bengal

Because there are permanent and strong radio-frequency interference sources around the coasts of Asia, SSS measurements from SMOS and Aquarius are likely to be of a lower quality in the Bay of Bengal. However, the paucity of *in situ* measurements in the Bay of Bengal in the satellite salinity era makes comparison difficult. The Bay of Bengal *in situ* A_T data measured in 2014 were not included in the main analysis due to their proximity to the coast (and so were removed due to the masking), and their inclusion causes the RMSDe of HG2 to increase to over $600 \mu\text{mol kg}^{-1}$ (Fig. S1). This demonstrates the importance of comparing like with like when evaluating the outputs and also highlights the influence of focusing on evaluation data without terrigenous influence. The low number of *in situ* data points used in the Bay of Bengal accuracy assessment highlights that the evaluation of output datasets (from both satellites and re-analysed *in situ*) will be biased against small-scale variability that may be captured by the *in situ* observation data used for the evaluation, particularly when *in situ* validation sites are relatively near-shore and the effect of riverine water flow is more pronounced. This was the case for the 2014 *in situ* dataset that was omitted from the main accuracy assessment due to falling within the masked area: the site was part of the Sundarbans Biological Observatory Time Series, representing the coastal part of the Sundarbans mangrove ecoregion, which can act as a source and a sink of CO_2 during pre-monsoon (April–May) (Akhand et al., 2017), and it is also an area that receives high freshwater discharge ($\sim 42000 \text{ m}^3 \text{ s}^{-1}$) along with local heavy seasonal precipitation, in addition to increasing anthropogenic pressure (Choudhury et al., 2015). The other case study regions have more data available for comparison and therefore this variability may be averaged out in the *in situ* data binning process. It is essential that more *in situ* carbonate system data are collected to elucidate these issues for this complex region (the Bay of Bengal), which has a strong riverine influence, and to characterise the variability on a wider scale than has currently been observed (Sarma et al., 2012; Samanta et al., 2015).

A large area of the Bay of Bengal is characterized by pCO_2 levels far

below the atmospheric value (i.e. a large gradient between atmospheric and oceanic $p\text{CO}_2$), which is more prominent during the north-east monsoon when the air-sea $p\text{CO}_2$ gradient exceeds $100 \mu\text{atm}$ (Akhand et al., 2013; Ganguly et al., 2011). The enhanced gradient is possibly due to new biological production sustained by excessive nutrient inputs from the Ganga-Brahmaputra-Meghna river basins, thus influencing the carbonate system via net organic production. Additionally, the presence of non-carbonate alkalinity in these regions (e.g. riverine contributions of organic species including humic acid) can result in A_T that is not correlated with salinity (Akhand et al., 2013). Only 14 of the outputs overlapped in space and time with the 2014 *in situ* data that captured this very near-shore variability, resulting in the apparent poor performance of these 14 outputs before coastal masking. If the other outputs had also captured this near-shore variability they may also have had reduced performance. Low satellite SSS coverage due to the issues of radio-frequency interference described above will have also contributed to lower performance of the satellite data driven outputs in this region. Improvements in satellite data coverage in coastal regions together with increased *in situ* data are likely to begin resolving these issues.

4.2. The need for continued efforts in quantifying uncertainties

The problem of uncertainties, and their propagation through the analysis, is an ongoing one. Here, the estimated uncertainties in the *in situ* measurements used for the evaluation and algorithm uncertainties were included in the analysis where they were quantifiable (i.e. nominal uncertainties for the C_T and A_T *in situ* evaluation measurements and the propagation of the empirical algorithm uncertainties). Published remote sensing uncertainties are available, however no such information exists for the other input datasets; and even within the carbonate system there are still many challenges to fully defining *in situ* and laboratory measurement uncertainties (Andrew Dickson, pers. comms.; Bockmon and Dickson, 2015). Therefore, quantification of associated uncertainties for all of the input data sources requires continued work. Furthermore, unavoidably in this analysis, data used to evaluate the algorithm outputs were unlikely to be wholly independent from the data used to create the algorithms. In order to have a fully independent evaluation dataset, original datasets would be required to develop the algorithms whilst keeping enough data separate from the algorithm development process to enable an independent evaluation. This was not possible in this initial assessment due to the general dearth of measurements in some regions, and due to ambiguity over which measurements were used to develop the historical algorithms.

However in relation to the calculated combined uncertainties of our outputs, the estimated combined uncertainties from Fine et al. (2017) of smaller than $\pm 20 \mu\text{mol kg}^{-1}$ for retrieving global A_T using satellite salinity and SST are consistent with our global results of RMSDe of $17 \mu\text{mol kg}^{-1}$, bias $< 5 \mu\text{mol kg}^{-1}$. This gives further confidence in the approach taken here. We note however that Fine et al., 2017 misinterpreted the uncertainty information provided by Olsen et al. (2016), as Olsen et al. only state the bias, which as previously discussed is only one component of a Type A uncertainty.

To test the sensitivity of the output uncertainties to the SST and SSS satellite remote sensing input data uncertainties, the latter were propagated through the analysis for all global empirical A_T algorithms (TS13, Lee06, Lee00, S13, S13g) for two example months (January and July). This results in A_T output uncertainties (due solely to satellite SSS and SST input data) of 0.2 to 0.8% (Table 6), which is close to the nominal *in situ* uncertainties of 0.5%, or $\pm 10 \mu\text{mol kg}^{-1}$. The combined uncertainty in most of the studied regions is considerably greater than this, implying that (in the global case at least) the other components of the uncertainty budget dominate over the remote sensing input data uncertainty.

4.3. The need for algorithm retraining and the collection of *in situ* observations

Only seven global and five regional algorithms were presented here, in addition to output of A_T and C_T from HG2, primarily because these were the only algorithms from the published literature that did not require additional re-parameterization for all the case study regions. Future efforts are needed to perform this re-fitting, not only for additional A_T and C_T algorithms, but also for the remaining carbonate system parameters ($p\text{CO}_2$ and pH). This is a demanding task; with just the 14 algorithms and model outputs used here, 1070 outputs were compared in the round-robin comparisons. Further, where few *in situ* measurements of a carbonate variable exist (e.g. pH), information could be obtained for future assessments by calculating this variable from two of the other carbonate variables (e.g. C_T and A_T) along with temperature and salinity. Calculating the variable in this way does introduce additional uncertainties, thus to be truly beneficial, such outputs should include the propagation of all uncertainties. A future assessment of the exploitation of satellite SSS will require further analysis of temporally resolved (rather than climatological) satellite observations, using new *in situ* data. We found only three cruises within GLODAPv2 that overlap with satellite salinity observations in our regions: none in the Bay of Bengal, one in the Amazon plume at the beginning of May 2010 (the first month of reliable SMOS data after its launch in November 2009) and two in the Amazon plume in April and May 2012 (shown in Figs. 8 and 9), one of which overlapped with the Greater Caribbean (only 6% and 3% of the GLODAPv2 data correspond to SMOS and Aquarius eras respectively). Hence coverage where we have both *in situ* and satellite observations is very limited spatially, seasonally and interannually, highlighting the need for further *in situ* data. It should also be noted that the lowest uncertainties achieved using these satellite observation-based and empirical approaches are still greater than the nominal *in situ* and laboratory measurement uncertainties (of $\pm 10 \mu\text{mol kg}^{-1}$) so the methods presented here are unlikely to ever be a substitute for *in situ* measurements. Their strength is in providing synoptic data to fill the inevitable gaps in the *in situ* data coverage. To enable all new *in situ* data to be fully exploited by the Earth observation community they need to have been collected following international protocols (as defined by Dickson et al., 2007), analysed using traceable standards (as advocated by Bockmon and Dickson, 2015) enabling the provision of a complete uncertainty budget (quantified as a Type A uncertainty, BIPM, 2008). If possible, the historical data contained within the GLODAPv2 dataset would benefit from the inclusion of some indication of their uncertainty budget e.g. a simple 'high', 'low' or 'unknown' determined using existing metadata and/or expert interpretation and opinion via a Type B uncertainty approach as defined by BIPM (2008). Similarly, the CORA re-analysis and WOA climatology data would benefit from similar additions as these datasets lack any uncertainty information.

4.4. Earth system model performance

It should be noted that we would not expect a free running global Earth system model such as HG2 to perform well regionally, though the poor global A_T performance and the relatively good performance in the Amazon plume were surprising. We include HG2 in the comparison mainly to illustrate how this methodology could be used to compare model data with quite different input sources such as satellite data. Our results provide a potentially useful dataset (including uncertainty information) to evaluate and challenge Earth system model outputs.

5. Conclusions

We demonstrate that satellite SSS and SST data are, in conjunction with empirical algorithms, able to successfully reproduce both A_T and C_T in four regions (globally, the Caribbean, the Amazon and the low salinity Amazon) as well as or better than *in situ*-derived (re-analysed)

SSS and SST using the same empirical algorithms, or a global Earth system model dataset, with the advantage that satellite datasets are acquired daily, on average, with synoptic coverage.

The ability to derive key surface carbonate system parameters from satellite observed SSS and SST offers the potential for quantifying natural variability, as well as monitoring the present state of these important parameters through space and time. Satellite sensors provide a significant advantage over traditional *in situ* derived climatologies because of the ability to provide synoptic and frequent observations of global oceans. Critically, many of the satellites that provide these data are already in operation, hence historic satellite sensor datasets could be used with these algorithms to elucidate changes over longer periods of time. These satellite methods should not replace ongoing *in situ* measurements, but should complement and enhance them by providing observations in periods where there are gaps in both time and space. Ongoing *in situ* data are essential to improve our ability to exploit satellite data, for example through enhanced parameterization of the algorithms. Satellites are also only able to measure surface waters, and are unable to measure under ice. These gaps must be filled with *in situ* data. Similarly, the evolving nature of the carbonate system due to anthropogenic forcing means that it is likely that these empirical algorithms will need to be periodically re-trained to maintain their performance. Hence the algorithms and methods utilized are useful for studying seasonal and inter-annual variations and episodic events, but may not be suitable for resolving longer-term trends.

The assessment presented here, which represents a significant effort and extensive analysis, provides the baseline performance against which any future algorithm re-training or re-calibration attempts can be compared.

Acknowledgments

This work was funded by the European Space Agency (ESA) Support to Science Element (STSE) Pathfinders Ocean Acidification project (contract No. 4000110778/14/I-BG, <http://www.pathfinders-oceanacidification.org/>) with additional support from the ESA Satellite Oceanographic Datasets for Acidification, OceanSODA, (contract No. 4000112091/14/I-LG, <https://www.esa-oceansoda.org/>). The authors thank Professor Andrew Dickson, Scripps Institution of Oceanography, for discussions about carbonate chemistry uncertainties and error propagation.

Appendix A. Supplementary data

Supplementary data to this article can be found online at <https://doi.org/10.1016/j.rse.2019.111469>.

References

Akhand, A., Chanda, A., Dutta, S., 2013. Characterizing air-sea CO₂ exchange dynamics during winter in the coastal water off the Hugli-Matla estuarine system in the northern Bay of Bengal, India. *J. Oceanogr.* 69, 687–697.

Akhand, A., et al., 2017. Potential CO₂ emission due to loss of above ground biomass from the Indian sundarban mangroves during the last four decades. *J. Indian Soc. Remote Sens.* 45 (1), 147–154.

Bates, N.R., et al., 2012. Detecting anthropogenic carbon dioxide uptake and ocean acidification in the North Atlantic Ocean. *Biogeosciences* 9, 2509–2522. <https://doi.org/10.5194/bg-9-2509-2012>.

BIPM, 2008. Evaluation of measurement data – guide to the expression of uncertainty in measurement. *JCGM* 100, 2008.

Bockmon, E.E., Dickson, A.G., 2015. An inter-laboratory comparison assessing the quality of seawater carbon dioxide measurements. *Mar. Chem.* 171, 36–43. <https://doi.org/10.1016/j.marchem.2015.02.002>.

Bonou, F.K., Noriega, C., Lefèvre, N., Araujo, M., 2016. Distribution of CO₂ parameters in the western tropical Atlantic Ocean. *Dyn. Atmos. Oceans* 73, 47–60. <https://doi.org/10.1016/j.dynatmoce.2015.12.001>.

Boutin, J., Martin, N., Reverdin, G., Yin, X., Gaillard, F., 2013. Sea surface freshening inferred from SMOS and ARGO salinity: impact of rain. *Ocean Sci.* 9, 183.

Boutin, J., et al., 2016. Satellite and *in situ* salinity: understanding near-surface stratification and subfootprint variability. *Bull. Am. Meteorol. Soc.* 97, 1391–1407.

Boutin, J., Vergry, J.L., Marchand, S., D'Amico, F., Hasson, A., Kolodziejczyk, N., Reul,

N., Reverdin, G., Vialard, J., 2018. New SMOS Sea Surface Salinity with reduced systematic errors and improved variability. *Remote Sens. Environ.* 214, 115–134. <https://doi.org/10.1016/j.rse.2018.05.022>.

Brix, H., Gruber, N., Keeling, C.D., 2004. Interannual variability of the upper ocean carbon cycle at station ALOHA near Hawaii. *Glob. Biogeochem. Cycles* 18. <https://doi.org/10.1029/2004GB002245>.

Bushinsky M., S., et al., 2019. Observing Changes in Ocean Carbonate Chemistry: Our Autonomous Future. *Current Climate Change Reports* 5 (3), 207–220.

Byrne, R.H., 2014. Measuring Ocean Acidification: new technology for a new era of ocean chemistry. *Environ. Sci. Technol.* 48 (10), 5352–5360.

Cabanes, C., et al., 2013. The CORA dataset: validation and diagnostics of *in-situ* ocean temperature and salinity measurements. *Ocean Sci.* 9, 1–18. <https://doi.org/10.5194/os-9-1-2013>.

Cai, W.-J., et al., 2010. Alkalinity distribution in the western North Atlantic ocean margins. *J. Geophys. Res.: Oceans* 115, n/a. <https://doi.org/10.1029/2009JC005482>.

Caldeira, K., Wickett, M.E., 2005. Ocean model predictions of chemistry changes from carbon dioxide emissions to the atmosphere and ocean. *J. Geophys. Res. Ocean.* <https://doi.org/10.1029/2004JC002671>.

Chao, Y., Farrara, J.D., Schumann, G., Andreadis, K.M., Moller, D., 2015. Sea surface salinity variability in response to the Congo River discharge. *Cont. Shelf Res.* 99, 35–45.

Choudhury, A.K., Das, M., Philip, P., Bhadury, P., 2015. An assessment of the implications of seasonal precipitation and anthropogenic influences on a mangrove ecosystem using phytoplankton as proxies. *Estuar. Coasts* 38, 854–872.

Cooley, S.R., Coles, V.J., Subramaniam, A., Yager, P.L., 2007. Seasonal variations in the Amazon plume-related atmospheric carbon sink. *Glob. Biogeochem. Cycles* 21, n/a. <https://doi.org/10.1029/2006GB002831>.

Del Vecchio, R., Subramaniam, A., 2004. Influence of the Amazon river on the surface optical properties of the western tropical North Atlantic ocean. *J. Geophys. Res.: Oceans* 109.

Dickson, A. G., Sabine, C. L., Christian, J. R. Guide to Best Practices for Ocean CO₂ Measurements, PICES Special Publication. (North Pacific Marine Science Organization, 2007).

Dickson G., A., Riley P., J., 1978. The effect of analytical error on the evaluation of the components of the aquatic carbon-dioxide system. *Marine Chemistry* 6 (1), 77–85. [https://doi.org/10.1016/0304-4203\(78\)90008-7](https://doi.org/10.1016/0304-4203(78)90008-7).

Drucker, R., Riser, S.C., 2014. Validation of Aquarius sea surface salinity with Argo: analysis of error due to depth of measurement and vertical salinity stratification. *J. Geophys. Res. Oceans* 119, 4626–4637.

Findlay F., H., et al., 2008. Carbon and nutrient mixed layer dynamics in the Norwegian sea. *Biogeosciences* 5 (5), 1395–1410. <https://doi.org/10.5194/bg-5-1395-2008>.

Fine, R.A., Willey, D.A., Millero, F.J., 2017. Global variability and changes in ocean total alkalinity from Aquarius satellite data. *Geophys. Res. Lett.* 44, 261–267. <https://doi.org/10.1002/2016GL071712>.

Friis, K., Körtzinger, A., Wallace, D.W.R., 2003. The salinity normalization of marine inorganic carbon chemistry data. *Geophys. Res. Lett.* 30. <https://doi.org/10.1029/2002GL015898>.

Ganguly, D., et al., 2011. Coupled micrometeorological and biological processes on atmospheric CO₂ concentrations at the land–ocean boundary, NE coast of India. *Atmos. Environ.* 45, 3903–3910.

Garcia E., H., et al., 2014a. World ocean atlas 2013. Volume 3, Dissolved oxygen, apparent oxygen utilization, and oxygen saturation, edited by: Levitus, S. A. Mishonov Technical Ed., NOAA Atlas NESDIS 75.

Garcia, H.E., et al., 2014b. World ocean atlas 2013. Volume 4, Dissolved inorganic nutrients (phosphate, nitrate, silicate), edited by: Levitus, S. A. Mishonov Technical Ed., NOAA Atlas NESDIS 76.

Gledhill, D.K., Wanninkhof, R., Millero, F.J., Eakin, M., 2008. Ocean acidification of the greater Caribbean region 1996–2006. *J. Geophys. Res.* 113, C10031. <https://doi.org/10.1029/2007jc004629>.

Gledhill, D.K., Wanninkhof, R., Eakin, C.M., 2009. Observing ocean acidification from space. *Oceanography* 22.

Ibáñez, J.S.P., Araujo, M., Lefèvre, N., 2016. The overlooked tropical oceanic CO₂ sink. *Geophys. Res. Lett.* 43, 3804–3812.

International Hydrographic Organization, 1953. 3 edn. Limits of Oceans and Seas, Special Publication 23 International Hydrographic Organization.

Jiang, Z.P., Tyrrell, T., Hydes, D.J., Dai, M., Hartman, S.E., 2014. Variability of alkalinity and the alkalinity-salinity relationship in the tropical and subtropical surface ocean. *Glob. Biogeochem. Cycles* 28, 729–742.

Johnson, K.S., Plant, J.N., Coletti, L.J., Jannasch, H.W., Sakamoto, C.M., Riser, S.C., Swift, D.D., Williams, N.L., Boss, E., Haëntjens, N., Talley, L.D., Sarmiento, J.L., 2017. J. Biogeochemical sensor performance in the SOCCOM profiling float array. *Geophys. Res. Ocean.* 122, 6416–6436. <https://doi.org/10.1002/2017JC012838>.

Jones, C.D., et al., 2011. The HadGEM2-ES implementation of CMIP5 centennial simulations. *Geosci. Model Dev.* (GMD) 4, 543–570. <https://doi.org/10.5194/gmd-4-543-2011>.

Kroeker, K.J., et al., 2013. Impacts of ocean acidification on marine organisms: quantifying sensitivities and interaction with warming. *Glob. Chang. Biol.* 19, 1884–1896. <https://doi.org/10.1111/gcb.12179>.

Lagerloef, G., Kao, H.Y., Meissner, T., Vazquez, J., 2015. Aquarius Salinity Validation Analysis; Data Version 4.0. Earth Space Res., Seattle, WA, USA.

Land, P.E., et al., 2015. Salinity from space unlocks satellite-based assessment of ocean acidification. *Environ. Sci. Technol.* 49, 1987–1994. doi:10.102/es504849.

Land, P.E., Findlay, H.S., Shutler, J.D., Ashton, I.G.C., Grouazel, A., Girard-Arduin, F., Reul, N., Piolle, J.-F., Chapron, B., Quilfen, Y., Bellerby, R.G.J., Bhadury, P., Salisbury, J., Vandemark, D., Sabia, R., 2019. Results and analysis of oceanic total alkalinity and dissolved inorganic carbon estimated from space borne, interpolated in

- situ, climatological and Earth system model data. PANGAEA. <https://doi.org/10.1594/PANGAEA.898115>.
- Le Vine, D.M., et al., 2014. Aquarius: status and recent results. *Radio Sci.* 49, 709–720. <https://doi.org/10.1002/2014RS005505>.
- Lee, K., Wanninkhof, R., Feely, R.A., Millero, F.J., Peng, T.H., 2000. Global relationships of total inorganic carbon with temperature and nitrate in surface seawater. *Glob. Biogeochem. Cycles* 14, 979–994.
- Lee, K., et al., 2006. Global relationships of total alkalinity with salinity and temperature in surface waters of the world's oceans. *Geophys. Res. Lett.* 33.
- Lefèvre, N., Diverrès, D., Gallois, F., 2010. Origin of CO₂ undersaturation in the western tropical Atlantic. *Tellus B* 62, 595–607. <https://doi.org/10.1111/j.1600-0889.2010.00475.x>.
- Lentz, S.J., Limeburner, R., 1995. The Amazon river plume during AMASSEDs: spatial characteristics and salinity variability. *J. Geophys. Res.: Oceans* 100, 2355–2375.
- Locarnini A., R., et al., 2013. World Ocean Atlas 2013, Volume 1: Temperature, edited by: Levitus, S. A. Mishonov Technical Ed., NOAA Atlas NESDIS 73.
- Merchant, C.J., et al., 2012. A 20 year independent record of sea surface temperature for climate from Along-Track Scanning Radiometers. *J. Geophys. Res.: Oceans* 117, 1978–2012.
- Merchant, C.J., et al., 2014. sea Surface temperature datasets for climate applications from phase 1 of the european space agency climate change initiative (SST CCI). *Geosci. Data J.* 1, 179–191.
- Millero, F.J., Lee, K., Roche, M., 1998. Distribution of alkalinity in the surface waters of the major oceans. *Mar. Chem.* 60, 111–130.
- Olsen, A., et al., 2016. The Global Ocean Data Analysis Project version 2 (GLODAPv2) – an internally consistent data product for the world ocean. *Earth Syst. Sci. Data* 8, 297–323. <https://doi.org/10.5194/essd-8-297-2016>.
- Osterman, G.B., Eldering, A., Avis, C., Chafin, B., O'Dell, C.W., Frankenberg, C., Fisher, B.M., Mandrake, L., Wunch, D., Granat, R., 2016. Orbiting Carbon Observatory-2 (OCO-2) Data Product User's Guide, Operational L1 and L2 Data Versions 7 and 7R. Jet Propulsion Laboratory, Pasadena, CA, USA.
- Perry, G.D., Duffy, P.B., Miller, N.L., 1996. An extended data set of river discharges for validation of general circulation models. *J. Geophys. Res.: Atmosphere* 101, 21339–21349.
- Raven, J.A., Caldeira, K., Elderfield, H., Hoegh-Guldberg, O., Liss, P.S., Riebesell, U., et al., 2005. Ocean Acidification Due to Increasing Atmospheric Carbon Dioxide 12/05 *The Royal Society*, Policy document.
- Reul, N., et al., 2012. Overview of the first SMOS sea surface salinity products. Part I: quality assessment for the second half of 2010. *IEEE Trans. Geosci. Remote Sens.* 50, 1636–1647.
- Reul, N., et al., 2014. Sea surface salinity observations from space with the SMOS satellite: a new means to monitor the marine branch of the water cycle. *Surv. Geophys.* 35, 681.
- Reul, N., Team, I.C.-C., 2015. SMOS Level 3 and 4 Research products of the Centre d'Expertise Ifremer du CATDS -Algorithm Theoretical Background Document. IFREMER-CNES technical document < <https://www.catds.fr/> > (2015).
- Salisbury, J., et al., 2011. Spatial and temporal coherence between Amazon River discharge, salinity, and light absorption by colored organic carbon in western tropical Atlantic surface waters. *J. Geophys. Res.: Oceans* 116.
- Salisbury, J., et al., 2015. How can present and future satellite missions support scientific studies that address Ocean Acidification? *Oceanography* 28, 108–121. <https://doi.org/10.5670/oceanog.2015.35>.
- Samanta, S., Dalai, T.K., Pattanaik, J.K., Rai, S.K., Mazumdar, A., 2015. Dissolved inorganic carbon (DIC) and its $\delta^{13}C$ in the Ganga (Hooghly) River estuary, India: evidence of DIC generation via organic carbon degradation and carbonate dissolution. *Geochem. Cosmochim. Acta* 165, 226–248.
- Santana-Casiano, J.M., González-Dávila, M., Rueda, M.J., Llinás, O., González-Dávila, E.F., 2007. The interannual variability of oceanic CO₂ parameters in the northeast Atlantic subtropical gyre at the ESTOC site. *Glob. Biogeochem. Cycles* 21. <https://doi.org/10.1029/2006GB002788>.
- Sarma, V.V.S.S., et al., 2012. Sources and sinks of CO₂ in the west coast of Bay of Bengal. *Tellus B* 64, 10961. <https://doi.org/10.3402/tellusb.v64i0.10961>.
- Sasse, T.P., McNeil, B.I., Abramowitz, G., 2013. A novel method for diagnosing seasonal to inter-annual surface ocean carbon dynamics from bottle data using neural networks. *Biogeosciences* 10, 4319.
- Smith, S.V., Key, G.S., 1975. Carbon dioxide and metabolism in marine environments. *Limnol. Oceanogr.* 20, 493–495.
- Takahashi, T., Sutherland, S., 2013. Climatological mean distribution of pH and carbonate ion concentration in Global Ocean surface waters in the Unified pH scale and mean rate of their changes in selected areas. Report No. OCE 10-38891. National Science Foundation, Washington, D. C., USA.
- Takahashi, T., et al., 2009. Climatological mean and decadal change in surface ocean pCO₂ and net sea-air CO₂ flux over the global oceans. *Deep-Sea Res. Pt II* 56, 554–577. <https://doi.org/10.1016/j.dsr2.2008.12.009>.
- Taylor, 1997. An Introduction to Error Analysis the Study of Uncertainties in Physical Measurements, second ed. University Science Books.
- Ternon, J.F., Oudot, C., Dessier, A., Diverres, D., 2000. A seasonal tropical sink for atmospheric CO₂ in the Atlantic ocean: the role of the Amazon River discharge. *Mar. Chem.* 68, 183–201. [https://doi.org/10.1016/S0304-4203\(99\)00077-8](https://doi.org/10.1016/S0304-4203(99)00077-8).
- Yang, D., Liu, Y., Cai, Z., Chen, X., Yao, L., Lu, D., 2018. First global carbon dioxide maps produced from TanSat measurements. *Adv. Atmos. Sci.* <https://doi.org/10.1007/s00376-018-7312-6>.
- Zweng M., M., et al., 2013. World ocean atlas 2013. Volume 2, Salinity. A. Mishonov Technical Ed., NOAA Atlas NESDIS 74.